Microglial reprogramming by Hv1 antagonism provides protection from inflammatory neurotoxicity

Diego Rolando Hernández-Espinosa (dih34@pitt.edu)
University of Pittsburgh https://orcid.org/0000-0002-2459-6422
Jenna R. Gale
University of Pittsburgh School of Medicine
Mia G. Scrabis
University of Pittsburgh Dietrich School of Arts and Sciences
Elias Aizenman
University of Pittsburgh School of Medicine

Research article

Keywords: Microglial activation, inflammatory neurotoxicity, voltage-gated proton channel, Hv1, metabolic reprogramming, excitotoxicity, neuroprotection

Posted Date: April 12th, 2022

DOI: https://doi.org/10.21203/rs.3.rs-1527316/v1

Abstract

Background

The precise mechanisms determining the neurodestructive or neuroprotective activation phenotypes in microglia remain unknown. Emerging evidence suggest, however, that metabolic changes are important for microglial phenotype determination. Metabolism, in turn, can be tightly regulated by changes in intracellular pH. The aim of this work was to establish whether pharmacological targeting of the microglial voltage gated proton channel 1 (Hv1), an important regulator of intracellular microglial pH, is critical for reducing inflammatory neurotoxicity while maintaining the neuroprotective components of activation, as well as to describe the mechanism behind this process.

Methods

We used lipopolysaccharide/gamma interferon (LPS/IFNγ) to activate a microglial cell line and primary microglia isolated from mouse and established the activation profile in the absence and presence of pharmacological Hv1 inhibition. Additionally, we utilized co-cultures of microglia and cortical rat neurons to assess the role of Hv1 in inflammatory neurotoxicity and the modulation of excitotoxic injury using a range of neuronal viability assays.

Results

Activation with LPS/IFNγ induced widespread production of proinflammatory mediators, as well as reactive species and phagocytic activity. The ensuing neurotoxicity was mainly attributable to the release of tumor necrosis factor alpha (TNFα), reactive oxygen species and zinc. Strikingly, pharmacological inhibition of Hv1 largely abrogated inflammatory neurotoxicity not only by reducing the production of cytotoxic mediators, but also by promoting neurotrophic molecule production and restraining phagocytic activity. Furthermore, we demonstrate that this Hv1-mediated change from a pro-inflammatory to a neuroprotective phenotype is associated with metabolic microglial reprogramming. Finally, we show that Hv1 antagonism not only reduces inflammatory neurotoxicity, but also promotes neuroprotection against excitotoxic injury.

Conclusions

We present a comprehensive characterization of the molecular components that are modulated by Hv1 activity during microglial activation in both a cell line and in primary microglial cells. Moreover, we show that Hv1 antagonism retains the beneficial aspects of microglial activation, not only by reducing inflammatory neurotoxicity, but also by providing neuroprotection in an *in vitro* model of excitotoxicity.

Our results suggest that Hv1 blockers are likely to provide an important therapeutic tool against a wide range of inflammatory neurodegenerative disorders.

Background

Microglia are the immune response orchestrator cell of the nervous system[1]. They detect changes in the microenvironment and produce a response that aims to recover tissue homeostasis[2]. These changes can be induced by pathogens or direct damage to neurons, both by physical and chemical means, resulting in microglia activation. This process is characterized by changes in protein expression and intermediary metabolism[3].

Microglial activation is highly regulated. Classically, the activation spectrum can be divided into two main phenotypes, one pro-inflammatory (M1) and the other anti-inflammatory (M2)[4], although intermediate phenotypes can exist between these two extremes[5,6]. During proinflammatory activation, microglia increase the production of recognition membrane molecules and reactive species production, while sustaining an elevated phagocytic activity[7,8]. Additionally, this response is characterized predominantly by the release of cytotoxic cytokines[9,10]. Although the production of these mediators is necessary for damage containment, sustained proinflammatory activation can, and often does, lead to widespread neuronal death[11], a process we define here as *inflammatory neurotoxicity*. In contrast, anti-inflammatory microglial activation is characterized by moderated phagocytic activity and enzymatic reactive species production, and, importantly, by the release of neurotrophic cytokines[12,13]. These effects promote neuroprotection as well as recovery of damaged neurons and thereby, tissue function[14,15]. Of note, microglial can oscillate between pro-inflammatory and anti-inflammatory phenotypes[16,17]. While a variety of conditions and molecules associated with both neurotoxic and neuroprotective profiles have been idetified[18], the precise mechanisms that regulate and determine the characteristics of the microglial response remain poorly defined.

Recently, microglial metabolism has emerged as a possible key regulator of microglial activation[19,20]. Intermediary metabolism, in particular, is closely related to activation phenotype determination, as increases in protein expression, reactive species formation, and cytokine production, increase cell energy demand[21]. During proinflammatory activation, microglia tend towards anaerobic metabolism, reflected by an increase in glycolytic rate, lactic acid production, and a decline in oxidative phosphorylation[22,23]. High lactate production and a decrease in reduced nicotinamide adenine dinucleotide (NADH), due to enhanced anaerobic glycolysis, can reduce the efficiency of antioxidant systems and glutamate reuptake[24,25].

Although anti-inflammatory activation is also characterized by cytokine production and enhanced phagocytic activity, these processes occur to a less significant degree and therefore demand fewer changes in energy metabolism[26]. The energy required by anti-inflammatory activation can be supplied by

oxidation of other energy substrates and via oxidative phosphorylation, without a significant increase in glycolysis and therefore, from lactic acid fermentation[16,27].

A common ground in which metabolic changes and microglial activation overlap is the regulation of intracellular pH[28]. Indeed, recent studies have strongly suggested that protons could be key regulators of the inflammatory response. For instance, extracellular acidification is associated with an increase in tissue injury in models of spinal cord injury and stroke[29,30]. In contrast, intracellular proton concentration has been shown to be correlated with reactive oxygen species production, phagocytic activity, as well the release of cytokines in immune cells[28,31], parameters that have a profound influence on the microglial response to injury.

Microglial activation is associated with a rise in proton production[32,33] due to the activity of reduced nicotinamide adenine dinucleotide phosphate (NADPH) oxidase 2 (NOX2). This increase in NOX2 activity, characteristic of proinflammatory activation, is essential to maintain phagocytosis and the subsequent respiratory burst[34]. Furthermore, NOX2 actively participates in the regulation of the inflammatory response through NFκB[35]. Upon activation, NOX2 transports an electron from NADPH to molecular oxygen to produce and extrude superoxide[36,37]. Without compensatory proton movement, the activity of this transmembrane electron transport would be sufficient to generate pronounced membrane depolarization as well as intracellular acidification[38].

Recent evidence points to Hv1 as an essential membrane proton channel for NOX2 function and microglial pH regulation[39,40,41]. This highly zinc-sensitive channel consists of two identical subunits that gate cooperatively[42–44]. Each subunit contains four transmembrane helices, S1–S4, which form a voltage sensitive domain (VSD)[45]. Hv1 extrude protons from activated cells to compensate for charge and osmotic imbalances due to NOX2 activity and metabolism, normalizing intracellular pH and regulating protein function. Although the absence of Hv1 does not significantly modify the physiology of non-activated microglia, during activation, a lack of Hv1 is associated with critical changes in the inflammatory response during damage to the nervous system[29,41]. Although these changes have largely been associated with a neuroprotective profile[46,47], the molecular mechanisms behind this process have largely remained undefined.

The majority of evidence about the neuroprotective effect associated with Hv1 lack of function has been obtained using knockout animal models[29,48]. However, selective pharmacological tools are available, including guanidine derivatives (i.e., 2-guanidinobenzimidazole, 2GBI and 5-chloro-2-guanidinobenzimidazole, ClGBI)[49] or arginine mimetics (i.e. 3-(2-amino-5-methyl-1H-imidazol-4-yl)-1-(3,5-difluorophenyl) propan-1-one, HIF and 2-aminobenzimidazole, ABI)[50], which have proven to be effective inhibitors in *in vitro* models of canine myocytes, human chorion-derived mesenchymal stem cells and Jurkat T cells (cells that functionally express the channel), as well as Xenopus oocytes expressing human Hv1 channels[50–53]. Guanidine derivatives, specifically ClGBI, are effective inhibitors at low micromolar concentrations, with low toxicity. Computational models also predict high membrane permeability [50,54].

Of interest, their chemical properties allow them to interact with voltage-gating domains, even when the Hv1 channel is in its closed conformation[45,49].

The purpose of the experiments described here was to define the molecular components of inflammatory microglial activation that are dependent on Hv1 function using a pharmacological blocker of the channel in two microglial preparations. Further, we sought to explore the metabolic changes and reprogramming characteristics induced by the pharmacological inhibition of the proton channel following activation. Our overarching goal is to provide evidence that Hv1 block can effectively lead to changes in microglial metabolic profile that result in neuroprotection, rather than only inflammatory neurotoxicity mitigation.

Materials And Methods

Experimental model and subject details

HAPI cell line

Rat immortalized microglia (Highly Aggressive Proliferating Immortalized or HAPI) cells were generously donated by Dr. J. Connor (Pennsylvania State University, Hershey, PA, USA). Please note that this cell line can now be purchased from EMD Millipore (#SCC103). HAPI cells were cultured in DMEM + GlutaMAx (Thermofisher, #10566016) containing 10% heat-inactivated fetal bovine serum (FBS; Thermofisher, A4766801), 100 units/ml penicillin G and 0.1 mg/ml streptomycin in a humidified 5% CO_2 incubator at 37°C. After reaching approximately 80% confluence, the cells were seeded at a density of 350,000 cells/ml and experimentally treated after 24 h[55].

Rat cerebrocortical neuronal cultures

For neuronal viability experiments, cultures were prepared from embryonic day 16 (E16) Sprague–Dawley rat cortices of either sex (Charles River Laboratories, Wilmington, MA, USA), as described previously[56]. Pregnant donor rats were euthanized by CO_2 inhalation. Cortices were dissociated with trypsin (0.6 mg/ml), and suspended in growth medium, composed of a v/v mixture of 80% Dulbecco's modified minimal essential medium, 10% Ham's F12-nutrients, and 10% bovine calf serum. Density was adjusted to 350,000 cells per well and plated on poly-l-ornithine–coated glass coverslips in six-well plates. Non-neuronal cell proliferation was inhibited after 14 days in vitro (DIV) with 2 μM cytosine arabinoside, and growth medium was changed to one consisting of Dulbecco's modified minimal essential medium and 2% bovine calf serum until cultures were utilized at 21 DIV[56].

Primary microglia culture: Microglia cultures were prepared from cerebral cortices of 1-day-old C57BL/6 mice of either sex (Charles River, Laboratories, Wilmington, MA, USA). After mechanical and chemical dissociation, cortical cells were seeded in DMEM-F12 with 10% FBS, 100 units/ml penicillin G, 0.1 mg/ml, and microglia supplement (Cell biologics, M1286) at a density of 250,000 cells/ml (62,500 cells/cm^2) and cultured at 37°C in humidified and 5% CO_2. Medium was replaced every 4 days and confluency was

achieved after 12–14 DIV. Microglia were separated by a 15-min incubation with a mild trypsin solution (0.25% trypsin, 1 mM EDTA) diluted 1:4 in DMEM-F12. Twenty-four hours after trypsinization, the isolated cells were fixed and immunostained, showing that the majority (97–99%) were positive for the specific microglial marker Iba1[57].

Microglial activation protocol

Twenty-four h post-seeding, both HAPI cells and primary microglia cultures were treated with a combination of LPS (1 mg/ml; Millipore, L4516) and IFNγ (0.1 mg / ml; Millipore, IF002) for 24 h to promote pro-inflammatory activation[58]. Activation was performed in both the absence and presence of Hv1 antagonism with ClGBI (Millipore, G11802). After 24 h of treatment, conditioned medium was obtained or activated cells were harvested to conduct the experiments described below.

Inflammatory neurotoxicity assessment

To establish the neurotoxicity effect of soluble molecules produced following microglial activation, coverslips from 21 DIV cortical cultures were transferred to 24-well plates and treated with 500 µl of conditioned medium from activated microglia[59]. Additionally, 2,2'-[1,2-Ethanediylbis(nitrilomethylidyne)] bis[6-methoxy-phenol manganese complex (EUK134; 100 µM; Millipore, #81065), dizocilpine hydrogen maleate (MK801; 10 µM; Millipore, M107), 2-pyridinylmethylamino ethylamine benzenesulfonic acid hydrate sodium salt (ZX1; 5 µM; Strem Co., #07-0350), TNF-α neutralizing antibody (nTNF-α; 10 µg/ml; Cell signaling, mAb11969), or IL-6 neutralizing antibody (nIL-6; 5 µg/ml; Invivogen #mabg-mil6-3) were co-administered to characterize the participation of the most widespread neurotoxic molecules of the proinflammatory activation. In co-culture experiments, microglia cultures were treated with LPS/IFNγ ± ClGBI for 24h as described above; after activation, cells were harvested (75,000 cells/ml in DMEM/F-12 medium) and plated directly on top of 21 DIV cortical cultures that had previously transfected with firefly luciferase-expressing plasmid for neuronal viability studies[60].

Excitotoxicity

To determine the effect of Hv1 inhibition on inflammatory neurotoxicity during excitotoxic damage, an *in vitro* model of glutamate reuptake inhibition was utilized [61]. Co-cultures of mixed cortical and microglia pretreated with LPS/IFNγ ± ClGBI, were expose for 24 h to DL-threo-β-Benzyloxyaspartic acid (TBOA), a glutamate transporter inhibitor, to induce neuronal excitotoxicity[62,63].

Viability assays

MTS assay protocol: Briefly, 20 µL of tetrazolium compound (3-(4,5-dimethylthiazol-2-yl)-5-(3-carboxymethoxyphenyl)-2-(4-sulfophenyl)-2H-tetrazolium), inner salt solution (MTS; 5 mg/ml; Abcam, ab223881) was added to cells in a 24-well plate and incubated at 37°C in a humidified 5% CO_2 incubator for 30 min. The resulting reduction of MTS tetrazolium compound by viable cells generates a colored formazan dye that is soluble in cell culture media[64]. The formazan dye was quantified by measuring the

absorbance (490–500 nm) using a microplate reader (Wallac 1420 Victor2 multilabel counter; PerkinElmer). Differences are expressed in percent of cell death against control.

MT-Luciferase assay: After analysis by MTS[65], cell viability was also evaluated in real time by using Real Time-Glo™ MT Cell Viability Assay (Promega Italia, MI). Briefly, cells were plated into 24-well plates, treated with LPS/IFNγ ± ClGBI and incubated for 24 h. After treatment, cells were incubated for 10 min with Real Time-Glo™ reagent, according to the manufacturer's protocol. Luminescence was measured using a microplate reader with an integration time of 0.5 s per well. In this assay, luminescent signal is correlated with the number of metabolically active cells. Results are provided as relative luminescence units (RLU; mean ± SEM of at least three independent experiments performed in triplicate).

LDH assay: LDH is rapidly released into the cell culture medium upon damage of the plasma membrane [60]. LDH release was determined using a commercial kit (Abcam, ab102526) following the manufacturer's instructions. Absorbance (490 nm) and background (690 nm) were measured. Results are calculated as background-subtracted absorbance measurements and expressed as normalized values against control (mean ± SEM of at least three independent experiments performed by triplicate or quadruplicate).

Co-culture neuronal viability assay: Neuronal cell death in neuron/microglia cocultures was measured using a luciferase activity assay[60,66]. For these experiments, we transfected neurons with a firefly luciferase-expressing plasmid (pUHC13-3 Luciferase, gift from Dr. H. Buchard) using Lipofectamine 2000 (Thermofisher, #11668030). Briefly, mixed coverslips with cortical cultures were transferred to a 24-well plate. Each well was transfected with 1.5 µg of DNA (25% firefly luciferase-pUHC13-3 and 75% pCDNA3 vector) in optiMEM (Thermofisher, #31985062). Twenty-four hours following transfection non-activated or activated microglia ± ClGBI (75,000 cells/ml) were plated directly on top on neurons[67]. Neuronal viability was assayed 24 h later using the Steadylite Plus Luminescence assay (PerkinElmer, #6016981). An overnight exposure to TBOA (75 µM; Tocris biotech, #1223) in the absence of microglia was used as a positive control for maximal neuronal cell death. Results are reported as percentage with respect to cortical neurons without treatment as control (mean ± SEM of at least three independent experiments performed by triplicate).

Immunoblotting

Cells were gently scraped off the wells on ice after being exposed to cell lysis buffer supplemented with a protease inhibitor cocktail (Millipore, #11697498). Debris was pelleted by centrifugation for 10 min at 8,000 rpm, and the remaining lysates were used immediately or stored at − 20°C. Protein concentrations of lysates were measured with a BCA assay (Thermofisher, #23225). Sodium dodecyl sulphate–polyacrylamide gel electrophoresis (SDS–PAGE) was conducted using the Mini Protean 3 System (Bio-Rad, Hercules, CA). Prior to electrophoresis, protein samples were treated with a reducing sample buffer and boiled at 100°C for 5 min. Samples with equal amounts of protein (30–50 µg per lane) were run on 8 or 12% SDS-PAGE gel for 2 h at 100 mV. For immunoblotting, separated protein bands were transferred onto a 0.25 µm nitrocellulose membrane (Bio-Rad) for 30 min at 18 mV in a semidry chamber. The membranes were then blocked with 3% fat free milk in PBS with 0.05% Tween 20 (PBST) at RT for 1 h

and probed with anti-gp91^{phox}(Abcam, ab129068), anti-NOS2 (Santa Cruz Bio., sc-7271), anti-Hv1 (Alomone labs. AHC-001) or anti-β-actin (Millipore, MAB1501) antibodies in PBST overnight at 4°C. After washing with PBST, blots were incubated with goat 680RD anti-Rabbit (1:10,000; Li-Cor, AB272118) or 800CW anti-Mouse (1:10,000; Li-Cor, AB2687825) at RT for 1 h. Blots were visualized using Odyssey Western blot detection system. Quantification was performed using ImageJ software (Wayne Rasband, NIH). Results were calculated as protein of interest/β-actin ratio and expressed as fold-change against normalized control (mean ± SEM of four independent experiments).

DHE stain and ROS detection

The cell permeable fluorescent dye dihydroethidium (DHE; Millipore, D7008) was used to detect intracellular ROS[68]. After 24h treatment of microglia with LPS/IFNγ ± ClGBI, DHE (5 μM) was added and incubated for 30 min at 37˚C and 5% CO_2. Cells were then washed and mounted on microscope slides. Images were obtained with a Nikon Eclipse Ti epifluorescence microscope (Nikon, Tokyo, Japan) using a 10X objective, and processed with NIS-Elements Advanced Research Imaging software (version 4.30.02, Nikon). In a separate set of experiments, cells were washed with PBS and MHB medium was added for direct quantification. Determination of final point DhE fluorescence was performed using a microplate reader at 610 nm when excited at 535 nm. Data is expressed in relative fluorescence units (RFU; mean ± SEM of at least three independent experiments performed by triplicate).

Immunofluorescent staining and image analysis

Cells were fixed with ice-cold ethanol for 5 min, washed with PBS and incubated with blocking solution, 1% Bovine serum albumin (BSA) and glycine 0.5% in PBST, for 30 min at RT. Next, cells were incubated with anti-Iba1 (1:200; Alomone, ACS-010)[69] overnight at 4°C. On the following day, the cells were incubated for 1h at RT with secondary antibody goat anti-rabbit conjugated with Alexa Fluor 488 (1:10000; Abcam, ab150077). DAPI (1:1000 in mounting solution) was used to stain the nucleus. For negative controls, cells were stained with the secondary antibody only. Fluorescent images were obtained at 10X and 40X magnification and analyzed as described above.

Microglial phagocytic activity

Phagocytic activity assay was measured according to the kit manufacturer's instructions (Abcam, ab235900)[70]. Briefly, cells were seeded in 96-well plates at a density of 250,000 cells per ml. After 24 h of LPS/IFNγ treatment, the medium was removed, and the assay buffer was added and incubated for 4 h. Following incubation, a quenching solution is added, and the fluorescence intensity measured in a plate reader (Ex 490/ Em 520). Phagocytic activity was calculated according to the standard curve given by the manufacturer after subtracting the mean relative fluorescent units (RFU) of the negative controls. The results are expressed as normalized values with respect to the control (mean ± SEM of at least three independent experiments performed by triplicate).

NOX activity

Microglial NOX activity was determined by a chemo-luminescent method[71]. Briefly, cells were harvested 24 h after treatments using a sterile cell scraper and 200 µL of ice-cold PBS. Subsequently, 100 µL of the sample (in duplicate) was transferred to a white microplate and 100 µM NADPH (Millipore, #2646711) and 100 µM lucigenin (Millipore, #2315971) were added. In parallel, 15 IU of superoxide dismutase (Millipore, #9054891) was added to a sample duplicate to subtract the unspecific oxidation. Additionally, samples were treated with DPI (100 µM; Millipore, D2926), a general inhibitor of NOX, or GSK-279 (1-100 µM; Millipore, SML2770) a specific inhibitor of NOX2 as negative controls. Luminescence was quantified using a plate reader. Values are expressed as relative light units (RLU) per mg protein (mean ± SEM of at least three independent experiments performed by triplicate).

NOS activity

Microglial nitric oxide synthase (NOS) activity was determined using an activity assay kit (Abcam, ab211083)[72]. Cells samples were prepared in ice-cold NOS kit assay buffer and centrifuged for 10 min at 10,000×g. Supernatants were collected, and protein concentrations determined by BCA assay. Samples were then incubated with NOS reaction mix for 1 h at 37°C. After incubation, NOS kit assay buffer and enhancer solution were added. This reaction mixture was incubated for 10 min at RT. For the color reaction, Griess Reagent was added. Absorbance was measured after a 10 min incubation by a microplate reader at 540 nm. NOS specific activity was then calculated from a standard curve and expressed as mU/mg protein (mean ± SEM of at least three independent experiments performed by triplicate).

Fluorometric pH_i and pH_e measurements

Intracellular pH (pH_i) was measured using cell-permeant BCFL-AM (Millipore, MAK150)[73]. Cells were seeded in 96 wells plates (500,000 cell per ml) and treated for 24 h. The medium was replaced with reaction solution (BCFL-AM and 50 mM Probenecid, in Hank's Buffer with 10 mM HEPES (HHBS). After, cells were then incubated at 37°C in an atmosphere of 5% CO_2 for 30 min while protected from light. Measurements were then performed at Ex 490 nm/ Em 535 nm in a microplate reader. The change in pH was corroborated by the addition of NH_3 (acid load) which promotes a decrease in intracellular pH and therefore, of fluorescence, followed by a slow and progressive recovery of the signal. The RFU value was equated to the pH scale by creating a curve of increasing concentration of BCFL-AM in HHBS, in which the pH was directly measured using a potentiometer (LabX, Corning 240). For the determination of extracellular pH (pH_e), culture medium was removed after the treatments and BCFL-AM was added to this solution, in the absence of cells. Medium was then incubated at 37°C in an atmosphere of 5% CO_2 for 30 min (protected from light). Following incubation, measurement was performed at Ex 490 nm/ Em 535 nm in a microplate reader. The fluorescence obtained was corroborated using a potentiometer (LabX, Corning 240) and reported as pH value mean ± SEM of at least three independent experiments performed by triplicate.

Metabolite determination

Lactate: Lactate production was measured by its oxidation coupled to NADH production, which, in turn, was detected via bioluminescence using a reductase/luciferase system assay kit (Promega, J5021)[74]. Briefly, microglia were seeded at 250,000 cells per ml into a 24 well plate and treated with LPS/IFNγ ± ClGBI for 24h. After the treatments, medium was removed and cells were incubated for 60 min with the reaction mix (luciferin detection reagent, NAD, lactate dehydrogenase, reductase, and reductase substrate). At the same time, medium was collected and treated with inactivation and neutralization solutions to inactivate the endogenous LDH and prevent NADH degradation for the extracellular measurement. RLU obtained are directly proportional to the lactate concentration following the production of a standard curve provided by the manufacturer. The total lactate was obtained by the sum of the lactate concentration in the samples and in the medium. Results are expressed as final lactate concentration (µM) and reported as mean ± SEM of at least three independent experiments performed by triplicate.

NAD+/NADH ratio: NAD levels were analyzed by use of the colorimetric total NAD+/NADH assay (Abcam, ab186032) that allows the differentiation of NAD^+ and NADH[75]. The assay reagent consisted of a mixture of NAD^+-reducing and NADH-oxidizing enzyme causing an amplification of the NAD signal. As NAD^+ but not NADH is heat labile at 60°C, total NAD is detected in the unheated sample and NADH is detected in the heated sample. The difference between total NAD and NADH represents NAD^+. One half of the samples was heated at 60°C for 30 min, while another half was kept on ice. A total of 40 µl of the unheated or heated samples as well as NADH (0.1–5.0 µM dissolved in PBS) were transferred to a clear 96-well microplate. After adding 40 µl of the enzyme reaction mix the color of produced formazan was measured at 450 nm in plate reader. Pure NAD^+ (Millipore, N0632) and NADH (Millipore, N8129) were used as reference standards. NADH can be detected at 260 and 340 nm, while NAD + is detectable at 260 nm only. Results are expressed as NAD^+ and NADH concentrations, normalized to control values (mean ± SEM of at least three independent experiments performed by triplicate).

Zinc measurements

FluoZin-3-Tetrapotassium salt (Thermofisher, F24194) was used as fluorescent indicator for extracellular Zn^{2+}[76]. All solutions used in these experiments were prepared with Milli-Q water previously treated with Chelex 100 (BioRad, #1422822), a chelating resin, to avoid metal cross-contamination. Briefly, after 24 hours of treatment, 200 µL of culture medium from the microglia cultures was transferred to a 96-well multiplate. Fluozin-3 (2µM) was immediately added to the samples and then incubated for 60 min at RT in the dark. Finally, the fluorescence resulting from the binding of Fluozin-3 to chelatable zinc was quantified in a multiplate reader (Ex: 485nm /Em: 535nm). Results are expressed as zinc concentration in µM, obtained from a curve of known concentrations of $ZnCl_2$ versus fluorescence and reported as mean ± SEM of at least three independent experiments performed by triplicate.

Hv1 knock down

HAPI cells were seeded and incubated until reaching at 50% confluence. Next, cells were transfected with Hv1 SMARTPool siRNA (Horizon, L-081118-02-0010) or the negative scramble control (SC; 100 nM;

Horizon, D-001210-02-20) using DharmaFECT 4 Transfection Reagent (Horizon, T-2004-03), according to the manufacturer's protocol. Additionally, a siRNA concentration curve (25–125 nM) was performed, and the effective concentration of siRNA was established (100 and 125 nM). Effective concentration was defined as a decrease of more than 80% in the amount of protein 48 h after transfection. The effectiveness of the siRNAs in suppressing Hv1 expression were determined by western blotting using anti-Hv1 antibody as described above.

Quantification and statistical analyses

Numeric values displayed represent the mean ± SEM of at least four independent experiments, each performed in triplicate. Graphs comparing values across groups were analyzed via one-way ANOVA with Tukey post-hoc analysis for individual comparisons. Unspecified comparisons are vs. control. Unspecified comparisons in normalized controls were separately analyzed via one sample t tests vs. 1. Significance is shown as $^{**}p < 0.05$, ** $p < 0.01$, *** $p < 0.005$ and **** $p < 0.001$.

Data availability

Any information required to reanalyze the data reported in this paper is available from the corresponding authors upon request.

Results

Well-tolerated Hv1 pharmacologic inhibition hampers the inflammatory activation profile of microglia. Experiments were performed both on HAPI cells and primary microglia cultures, which both express Hv1 (Fig. S6). We first sought to characterize the main response properties of HAPI cells upon activation by LPS/IFNγ and to determine whether any of these responses would be altered by the presence of an Hv1 antagonist. HAPI cells were first exposed to increasing concentrations of LPS (0.25-5 mg/ml) in the presence of 0.1 mg/ml IFNγ for 24 hours. We note that concentrations higher than 0.5 mg/ml of LPS (with 0.1 mg/ml IFNγ) reliably increased all inflammatory activation parameters measured (Fig. S1), consistent with an M1 phenotype. We next established the maximal concentration of an Hv1 antagonist these cells could tolerate without observable cell death (Fig. S2). Cell death was quantified using MTS and LDH assays during both basal and activated conditions (1 mg/ml LPS/0.1 mg/ml IFNγ) 24 hours after exposure to increasing concentrations (5–20 μm) of ClGBI, an Hv1 blocker. ClGBI is highly efficacious (~ 90% channel block) and the most potent (EC50 = 1 μM) of the guanidine-derived antagonists of the proton channel[49]. We observed that 10 μM of the blocker was well-tolerated without any observable cell death in both non-activated and activated HAPI cells (Fig. S2 A-D). Next, using the MT-luciferase assay, we monitored the long-term viability of non-activated and activated HAPI cells that had been exposed to vehicle or 10 μM ClGBI for 24 h. Interestingly, no apparent long-term impact of Hv1 antagonism was observed in non-activated or activated cells after 72 hours after treatment. In the next set of experiments, we use the same approach in primary microglia cultures obtained from postnatal mouse brain. For these studies, we first evaluated the sensitivity of these cells to the presence of increasing concentrations of ClGBI, similar to the characterization performed in HAPI cells (Fig. S3). We

found that the primary microglia cultures could withstand 10-fold less the concentration of the antagonist when compared to our cell line, showing as clear decrease in viability when exposed to ClGBI concentrations higher than 1 μM for 24 hours, both under basal and activated (1.0 mg/ml LPS/0.1 mg/ml IFN) conditions (Fig. S3A-D). Additionally, we assessed the effect of treatments on the long-term viability of microglia cultures. We found that after 4 weeks, the viability of activated microglia decreases by 50%. Remarkably, co-administration of 1 μM ClGBI restores viability by 25% (Fig. S3E). Given these results, we chose to utilize 1 mg/ml/0.1 mg/ml IFNγ to activate both immortalized and primary microglial cells as well to utilize 10 μM ClGBI for HAPI cells and 1 μM ClGBI for primary microglia cultures to antagonize Hv1 in subsequent studies.

As our initial data suggested an increase in ROS production (S1B) after activation of HAPI cells, we quantified the protein expression levels of the main reactive species-producing enzymes during HAPI cell activation, namely NOX2 (Fig. 1A and S7A) and NOS2 (Fig. 1B and S7B). We found that following HAPI cell activation NOX2 protein was increased nearly two-fold (Fig. 1C). Importantly, the presence of ClGBI during activation attenuated this response although incubation with ClGBI alone had a small stimulatory effect (Fig. 1C). In the case of NOS2, activation produced a dramatic 60-fold increase in protein expression, while Hv1 inhibition during activation reduced NOS2 expression to approximately half this level (Fig. 1D). ROS production itself was next evaluated utilizing DhE fluorescence, which detects superoxide and hydrogen peroxide (Fig. 1E). We observed a substantial increase in fluorescence in activated cells, which was significantly mitigated by ClGBI (Fig. 1F). Given that Hv1 antagonism reduced the expression of both NOX2 and NOS2 in activated cells, we hypothesized that the ClGBI-mediated decrease in reactive species production was due, in part, to a reduction in NOX and NOS2 enzymatic activity. Indeed, quantification of enzymatic activity revealed that while NOX activity increased threefold in response to activation, Hv1 inhibition completely suppressed this response (Fig. 1G and S4A). Additionally, activated cells showed a 20-fold increase in NOS2 activity, a phenomenon that was partially blocked by Hv1 inhibition (Fig. 1H). We next quantified phagocytic activity to establish whether this important activation parameter could also be regulated by Hv1 antagonism. After activation, HAPI cells more than doubled their phagocytic activity, while co-administration of ClGBI effectively limited this increase and returned it near baseline levels (Fig. 1I and S5B). Finally, we measured the extracellular concentration of zinc ($[Zn^{2+}]_e$) since macrophage response to LPS is associated with changes in zinc homeostasis[77]. We observed a significant increase in $[Zn^{2+}]_e$, secondary to the activation of HAPI cells, which was not modified by Hv1 antagonism (Fig. 1J). In sum, our data strongly suggest that HAPI microglial cells show a complete, general inflammatory pattern following activation. Furthermore, our data prove that Hv1 antagonism during activation can effectively hamper the extent of reactive oxygen and nitrogen species generated by limiting their enzymatic production. Importantly, while activation leads to enhance phagocytic activity, Hv1 antagonism in activated microglia dampens but does not eliminate this critical function of these cells.

Having established the inflammatory activation pattern of immortalized microglia cells and the extent to which Hv1 inhibition modifies key components of this phenotype, we next aimed to establish whether

primarily microglial cells responded similarly. We compared the expression levels of NOX2 (Fig. 2A and S7C) and NOS2 (Fig. 2B and S7D) in primary mouse microglial cultures at rest and following activation, both with and without Hv1 inhibition. We observed that ClGBI (1μM) alone could enhance NOX2 expression in non-activated microglia, and that activation could further enhance this process (Fig. 2C). Strikingly, activation in the presence of the Hv1 blocker depressed NOX2 expression levels well below control levels (Fig. 2C). Similar to the results obtained with HAPI cells, activation promoted a dramatic ~ 40-fold increase in NOS2 expression in primary microglial cells, a phenomenon that was attenuated by Hv1 inhibition (Fig. 2D). The changes in expression of these two proteins were paralleled by enhanced DhE staining in activated cells, with a concomitant decrease in staining in ClGBI-treated activated cells (Fig. 2E; quantified in Fig. 2F). NOX activity, NOS activity and phagocytosis followed a similar pattern to that observed in HAPI cells, with increased activity upon activation, as well as inhibition by Hv1 antagonism (Fig. 2G-I). Once again, activated cells retained phagocytotic capabilities near what is normally observed by non-activated microglia in the presence of ClGBI, (Fig. 2I). Activated microglia presented a similar increase in $[Zn^{2+}]_e$ to that observed in HAPI cells, while of greater magnitude. Upon activation, $[Zn^{2+}]_e$ concentration increased nearly three-fold, and this response was not attenuated by ClGBI treatment (Fig. 2J). Our findings suggest that ROS production and enhanced phagocytic activity are dependent on Hv1 activity and that its inhibition can have an important influence on their regulation. On the other hand, zinc release appears to be an activation parameter independent of Hv1 activity. Most importantly, the activation profile of HAPI cells appears to robustly reproduce what is normally observed in primary microglial cells making them a valuable tool in the study of brain inflammatory processes.

Hv1 block prevents proton extrusion and acidifies the intracellular pH of activated microglia. As Hv1 promotes proton extrusion in response to intracellular pH acidification, we next determined the impact of ClGBI on the intracellular (pH_i) and extracellular (pH_e) pH of HAPI cells, using BCFL-AM, an intracellular fluorescent indicator. First, we evaluated different concentrations of ClGBI (Fig. S4). Interestingly, we did not observe changes in pH_i or pH_e at any concentration of ClGBI tested (2.5–10 μM) on non-activated HAPI cells (Fig. S4A, B). However, following activation, a significant decrease in pH_i, as well as an increase in pH_e, was observed with 7.5–10 μM ClGBI (Fig. 3A, B; Fig. S4 C, D). These results indicate that activation leads to pronounced intracellular acidification and that Hv1 inhibition intensifies this effect. Moreover, this activation-induced intracellular acidification is associated with a decrease in proton extrusion, which can be measured by a change in pH_e. As such, both pH_i and pH_e can be modulated by Hv1 inhibition in activated cells. These findings are consistent with the known function of the proton channel during microglial activation[31,78] and are nicely recapitulated in our HAPI cell preparation. Finally, we confirmed that the activation and ClGBI-mediated changes in pH_i and pH_e observed in the cell line were also present in the primary microglial cells, which was indeed the case (Fig. 3C, D), further demonstrating the utility of HAPI cells as an excellent microglial cell line model.

NOX2 activity promotes intracellular acidification in activated HAPI cells. During microglial activation, ROS production by NOX2 results in a release of protons into the intracellular space. As such protons extrusion, particularly by Hv1, is necessary for maintaining electroneutrality. We investigated the impact

of NOX2 activity on pH_i using GSK279, a specific competitive inhibitor of NOX2[79]. As previously noted, treatment with LPS/IFNγ led to a four-fold enhancement of NOX activity in HAPI cells. In contrast, activation in the continuous presence of GSK279 (1-100 μM) led to a concentration-dependent inhibition of NOX activity, reverting to near control activity at the highest concentration of the inhibitor (Fig. 4A). As NOX2 activity likely leads to the aforementioned intracellular acidification following activation, we confirmed that GSK279 similarly led to a concentration-dependent reversal of pH_i changes observed in HAPI cells following treatment with LPS/IFNγ (Fig. 4B). Importantly, GSK279 could also effectively abrogate the enhanced acidification produced by Hv1 inhibition in activated cells (Fig. 4C). These results suggest not only that NOX2 is largely responsible for the intracellular acidification secondary to activation but that the functional coupling between Hv1 and NOX2 governs intracellular pH during the microglial inflammatory response. Moreover, the enhanced intracellular acidification as a result of Hv1 block in activated cells is the likely mechanism behind ClGBI-mediated inhibition of NOX2 activation[80].

Pharmacological inhibition of Hv1 modifies the activation metabolic profile. As intracellular acidification is associated with intermediary metabolism changes[81,82], we next measured critical parameters of metabolism under basal and activated conditions in our microglial cell line. First, we assessed intracellular lactate ($lactate_i$) concentrations, since proinflammatory microglial activation is associated with increased anaerobic glycolysis[82]. Intracellular lactate increased almost four-fold during activation, compared to control, a phenomenon that was significantly attenuated by ClGBI treatment (Fig. 5A). Additionally, activation not only promoted lactate production but also its release into the extracellular space. After 24 hours of treatment with LPS/IFNγ, the concentration of extracellular lactate ($lactate_e$) increased more than fifteen times baseline levels, which, again, was strongly inhibited by Hv1 block (Fig. 5B). These changes were also reflected by total lactate measurements (Fig. 5C). Subsequently, we investigated whether these metabolic changes would also be present in activated primary microglia cultures. The effects of activation and Hv1 blockade on the concentrations of $lactate_i$, $lactate_e$ and total lactate seen in HAPI cells were again reproduced in this system (Fig. 5G-I). This rise in lactate production is indicative of a metabolic shift toward anaerobic glycolysis in activated cells which negatively impacts energy production through oxidative phosphorylation[83].

An accurate indicative parameter of the energy status of cells is the oxidation state of NAD. A decrease in NAD^+/NADH ratio is generally associated with oxidative stress while increases in ratios are an indicator of metabolic stress[84]. Activated HAPI cells showed a moderate decrease in NAD^+ compared to non-activated cells, which could be completely prevented by Hv1 inhibition (Fig. 5D). Additionally, we found that activation dramatically decreased the concentration of NADH when compared to non-activated cells, an effect that was again mitigated by ClGBI (Fig. 5E). These changes in NAD^+ and NADH led to a 4-fold increase in the NAD^+/NADH ration upon activation, which was significantly attenuated by Hv1 antagonism (Fig. 5F). A nearly identical pattern of NAD^+ and NADH changes were observed in our primary microglia cultures (Figs. 5G-L). These results suggest that activation promotes lactate production and NADH consumption, processes directly associated with increased anaerobic glycolysis. The fact that Hv1

antagonism effectively prevents these metabolic changes in both cellular models indicates that inhibition of this voltage-gated proton channel may promote the conservation of a more favorable energy status.

Hv1 inhibition promotes an anti-inflammatory activation phenotype. As the microglial activation phenotype can be strongly influenced by metabolic changes[24,85], such as those promoted by Hv1 inhibition, we next characterized the secretome profile of both non-activated and activated HAPI cells and primary microglia in the presence and absence of ClGBI. To do so, we quantified the concentration of cytokines in the culture medium of cells in the aforementioned conditions. Interestingly, ClGBI alone moderately increased the production of IL-1β in non-activated HAPI cells, when compared to control. IL-1β levels were further increased in activated cells. However, in this case, Hv1 block did not modify the response (Fig. 6A). In contrast, ClGBI alone did not influence IL-1β production in non-activated primary microglia cultures, but it did significantly reverse the increased production of this cytokine in activated cultures (Fig. 7A). Both HAPI and primary microglial cell activation produced a robust increase in IL-6 production, with ClGBI co-treatment markedly inhibiting its production (Fig. 6B and 7B). A similar pattern was observed with TNFα production, and its inhibition by ClGBI, in both HAPI (Fig. 6C) and microglial cells (Fig. 7C). These results confirmed that upon activation both our models increase production of well-known pro-inflammatory cytokines, which are largely suppressed by Hv1 antagonism.

Given these findings and our data demonstrating that Hv1 hampers inflammatory activation (Figs. 1 and 2), we examined whether Hv1 could also promote an anti-inflammatory phenotype. We quantified three cytokines directly associated with anti-inflammatory responses in microglia, namely IL-4, IL-10, and TGF-β. HAPI and microglial cell activation was accompanied by a moderate decrease of IL-4, which was normalized to control levels by ClGBI in both cell types (Fig. 6D and 7D). In contrast to these observations, the patterns of IL-10 production differed between HAPI (Fig. 6E) and primary microglial (Fig. 7E) cells. In both cases, production of this neuroprotective cytokine increased upon activation. We observed a nearly 50% decrease in IL-10 levels in HAPI cells treated with ClGBI alone as well as a similar decrease in activated cells exposed to the Hv1 antagonist. In contrast, we did not observe a decrease in IL-10 in non-activated or activated primary microglial cells treated with ClGBI. TGF-β, a potent inducer of anti-inflammatory polarization[86], decreased following activation in both cell types. For this cytokine, we did not observe a significant rescue in production by ClGBI in neither HAPI nor microglial cells, although there was a trend towards recovery in the cell line model (Fig. 6F and 7F). These results suggest a complex effect of Hv1 inhibition on anti-inflammatory cytokine production in the cell line and primary microglia cultures. However, the general pattern observed is one in which an anti-inflammatory phenotype is maintained in activated cells when Hv1 is antagonized, favoring an IL-4 (and perhaps TGF-β)-favored neuroprotective profile in HAPI cells, and an IL-4/IL-10 profile in the mouse microglial cultures.

Finally, we examined the morphological changes associated with HAPI and microglial cell activation by means of Iba-1 labeling (Fig. 6G and 7G). Control non-activated HAPI cells generally presented a compact, uniform, and rounded soma, with few projections. This morphology appeared unaffected by the presence of ClGBI alone. After treatment with LPS/IFNγ, we observed an increase in the size of the soma, acquiring an irregular appearance. When activation occurred during Hv1 inhibition, cells exhibited both

types of morphology, although the vast majority resembled non-activated, inactivated cells. This morphology activation pattern suggests the acquisition of an alternative or mixed phenotype[87] under these conditions (Fig. 6G), which is consistent with their secretome profile. Similarly, to the cell line, ClGBI treatment in non-activated microglial cells did not change their morphology. However, after 24 hours of LPS/IFNγ treatment, we observed growth in the size of the soma and a reduction in the number of processes, correlating with a classic proinflammatory activation profile[87]. Treatment of activated microglia with ClGBI again resulted in a morphological profile more akin to the non-activated state (Fig. 7G).

Hv1 inhibition during activation reduces inflammatory neurotoxicity. The results presented thus far shown that Hv1 inhibition decreases the microglial production of reactive species and proinflammatory mediators, while promoting the release of anti-inflammatory cytokines. To determine the functional implications of these changes to the activation profile of microglia, we examined their neurotoxicity in the presence and absence of ClGBI. Rat cortical neuron cultures were exposed to conditioned medium from non-activated and activated HAPI and microglial cells treated with or without ClGBI. Twenty-four hours after exposure, neuronal viability was quantified by LDH and MTS assays. Cortical cultures exposed to medium harvested from activated HAPI (Fig. 8A), and microglial (Fig. 9A) cultures resulted in a significant loss of neuronal viability as evidenced by increased LDH release (Figs. 8A and 9A). Critically, we found that Hv1 antagonism with ClGBI during activation prevented the neurotoxicity of the conditioned medium (Figs. 8A and 9A). These findings were confirmed in the MTS assay (Fig. 8B and 9B). These data strongly suggest that in the presence of an Hv1 blocker, the secretion of neurotoxic factors by activated microglia is significantly attenuated.

Having demonstrated that Hv1 inhibition limits neurotoxicity associated with the release of pro-inflammatory mediators by activated microglia, we turned our focus to identifying the diffusible molecules that contribute to the observed neurotoxic profile in our models. As oxidative stress is closely related to inflammatory neurotoxicity[88], we first assessed whether antioxidant exposure could increase neuronal viability using the MTS assay. Indeed, EUK134 (100 μM), a synthetic superoxide dismutase/catalase mimetic[89], provided neuroprotection against toxicity associated with HAPI and microglial conditioned media exposure (Figs. 8C and 9C). Given that extracellular zinc is neurotoxic to our cortical cultures[90] and that we demonstrate that activation in both HAPI cells and microglia causes an increase in extracellular Zn^{2+}, we evaluated whether the extracellular zinc chelator ZX1[91] (5 μM) could provide some degree of neuroprotection to conditioned media exposure. Indeed, ZX1 treatment significantly increased neuronal viability in cortical cultures exposed to conditioned media from activated microglia (Fig. 8D and 9D). Finally, we used neutralizing antibodies to block the activity of IL-6[92] and TNFα[93], neurotoxic cytokines released during activation in both our models. Surprisingly, neutralization of IL-6 (5 μg/ml) was not sufficient to reverse the neurotoxicity induced by the conditioned media from either activated HAPI (Fig. 8E) or microglial (Fig. 9E) cultures. In contrast, we found that a TNFα neutralizing antibody (5 μg/ml) significantly increases the viability in both cases (Fig. 8F and 9F). Of note, none of the neuroprotective actions of EUK134, ZX1 or TNFα neutralization were additive with the previously noted

protective actions of ClGBI (Fig. 8C-F and 9C-F), suggesting that Hv1 block protects neurons, in part, by preventing sufficient pro-inflammatory cytokine production by activated microglial cells.

Hv1 inhibition promotes neuroprotection from microglia during excitotoxic damage. In the next set of experiments, we evaluated: *i)* whether co-cultures of microglia and cortical cells resulted in neurotoxicity following activation, *ii)* whether inducing excitotoxicity in neurons could itself result in microglial activation and further enhance neurotoxicity, and *iii)* whether Hv1 inhibition could restore neuronal viability following microglial activation and/or excitotoxic insults. In both our HAPI/cortical and microglia/cortical co-cultures we observed a 2-fold increase in LDH release following activation, indicating, once again, that microglial activation results in neurotoxicity (Fig. 10A, D). Importantly, in both cases, the presence of ClGBI abrogated the neurotoxicity (Figs. 10A, D). Since an elevated LDH could be reflective of the presence of both injured microglia (induced by dying neurons) and neurons, we took advantage of a luciferase viability assay in previously transfected neurons, which exclusively reflects neuronal viability in co-culture or mixed culture conditions[60,63]. Using this assay, we confirmed both a decrease in neuronal viability following microglial activation, as well as neuroprotection by Hv1 block (Fig. 10B, E).

We next explored whether microglia were protective against a canonical excitotoxic insult and whether Hv1 antagonism modified this response. We first exposed cortical cultures alone to the glutamate uptake inhibitor TBOA (75 μM), noting, as expected[62,63], a substantial decrease in neuronal viability, as measured by the luciferase assay (Fig. 10C). In the absence of HAPI cells, the observed excitotoxicity was not influenced by the presence of the Hv1 blocker. In contrast, when neurons were in co-culture with non-activated HAPI or microglial cells, TBOA toxicity could be partially ameliorated by ClGBI (Figs. 10C and 10F), suggesting that neuronal excitotoxic injury, in and of itself, is sufficient to trigger microglial cell activation, as observed in other systems[37]. Moreover, we observed increased TBOA toxicity when neurons were exposed to previously activated HAPI or microglial cells, but only when ClGBI was absent during activation. However, even under these circumstances ClGBI was protective if added during the TBOA exposure (Figs. 10C and 10F, right two sets of bar graphs). This critically important result indicates that Hv1 block not only prevents activated microglia neurotoxicity but also, by reprogramming these cells, Hv1 antagonism can generate an overall neuroprotective environment.

Discussion

We show that pharmacologic inhibition of Hv1 during proinflammatory activation decreases microglial neurotoxicity and promotes neuroprotection against excitotoxic damage. Hv1 antagonism decreases the enzymatic production of reactive species, mostly through inhibition of NOX2. Despite ClGBI marked effect on NOX2 activity, Hv1 antagonism only partially blocks NOS2 and phagocytic activity, which are processes associated with neuroprotection[94,95]. We also observed that the secretome of activated HAPI cells and microglia is characterized by a significant increase in proinflammatory cytokines (IL-1β, IL-6, and TNFα) and the reduction in anti-inflammatory cytokines (IL-4 and TGFβ). These described characteristics of this profile is consistent with what has been reported in various models of

proinflammatory activation[96,97]. Adding to this body of work, we report that Hv1 antagonism promotes a drastic change in the secretome, characterized by a decrease in the pro-inflammatory cytokines IL-6 and TNFα in both primary and immortalized microglia as well as a decrease in IL-1β in primary microglia. Importantly, Hv1 inhibition promotes an increase in the neurotrophic cytokine IL-4 in both systems as well as an increase in IL-10 in primary microglia. These changes to the microglia secretome following activation indicates that ClGBI promotes the acquisition of an anti-inflammatory phenotype by decreasing the production of proinflammatory factors and tilting the balance towards the release of neurotrophic cytokines.

Additionally, we assessed the neurotoxic capacity of the activated microglia secretome in cortical neurons and whether it was modified by Hv1 antagonism. We found that conditioned media from activated microglia was indeed neurotoxic, and this toxicity was mainly dependent on the release of TNFα, as well as to the production of ROS and the release of extracellular zinc. Surprisingly, Hv1 inhibition does not add to the neuroprotection provided by the neutralization of TNFα nor the use of an antioxidant or a zinc chelator, suggesting that, in fact, these are the activation changes promoted by Hv1 blockade that are associated with increased neuronal viability.

Hv1 normally extrudes protons to the extracellular space, a crucial process when metabolism and ROS production by NOX2 activity increase during activation[31,98]. In non-activated microglia, the intracellular pH does not fluctuate significantly, which keeps Hv1 in a closed state[99]. After activation, NOX2 activity increases, which causes a rapid increase in the intracellular proton concentration. This rise in intracellular proton concentration promotes increased activity of Hv1 in order to maintain microglial pH and electroneutrality[39,100]. We observed that ClGBI blocked proton outflow, inducing a greater intracellular acidification, while at the same time, preventing a decrease in extracellular pH. We posit that the decreased extracellular pH changes observed in our system after Hv1 inhibition contribute to the observed increased neuronal viability, as extracellular acidity can be neurotoxic[29]. Indeed, these pH changes are consistent with the neuroprotection observed in genetic models of Hv1 depletion[41].

Microglial activation is a rapid response that depends on a very flexible metabolism to satisfy the energetic requirements for surface marker expression and cytokine and reactive species production [83,101–103]. In this study we corroborate that activation promotes an increase in lactate production, which is most likely attributable to a boost in glycolytic rate. Increased lactate production is a common phenomenon in pro-inflammatory activation, and, in fact, high lactate concentration is associated with IL-6 and TNFα production[24,104,105]. We found an increased NAD^+/NADH ratio, which is directly associated with an increase in lactic fermentation. This metabolic shift is associated with a decrease in mitochondrial ATP production, and even mitochondrial dysfunction[106]. Importantly, Hv1 inhibition considerably decreases lactate production, as well as significant increases NADH. These changes are associated with a lower energy state, in which glycolytic ATP production and lactic fermentation decline[107]. Together, these findings strongly suggest that Hv1 blockage promotes microglial metabolic reprogramming during activation, a key component of its neuroprotective phenotype. It must be noted

that the loss of Hv1 function had previously been associated with the acquisition of anti-inflammatory responses associated to neuroprotection[108–111], albeit by an uncharacterized process, which we define here.

Finally, in this study we evaluate the impact of microglial reprogramming during excitotoxic damage. Our data suggest that non-activated microglia do not modify neuronal death during the excitotoxic event; however, when the microglia are previously activated, neuronal viability decreases significantly. This loss of neuronal viability in co-culture is likely due to the summative effect of inflammatory neurotoxicity and excitotoxic damage. Most importantly, our data show that when activation occurs during Hv1 inhibition, not only is inflammatory neurotoxicity prevented, but microglia are capable of protecting neurons against excitotoxic damage. Furthermore, Hv1 blockade in co-culture promotes neuroprotection even if the microglia were previously activated in the absence of Hv1 block.

Limitations of this study

In addition to the pharmacological inhibition of Hv1, we examined whether Hv1 silencing would result in a similar scenario. However, we found that although siRNA was effective in decreasing Hv1 expression in non-activated HAPI cells, this effect was lost in activated cells (Fig. S5B,D), possibly as a result of Hv1 membrane stabilization upon activation. It must be noted that this study does not take into account the potential role of astroglia, which are crucial intermediaries and amplifiers of cytokines action[112]. Additionally, we know that microglial metabolism is closely coupled to astrocyte and neuronal metabolism[103]. Finally, this approach has all the common limitations of *in vitro* models, so the validation of these results in an *in vivo* model is a priority of future work.

Conclusions

Our findings indicate that Hv1 pharmacological inhibition considerably reduces inflammatory neurotoxicity by promoting an anti-inflammatory secretome. We propose that the intracellular acidification of microglia, promoted by the Hv1 antagonism, decreases the energy demand of these cells, which, in turn, promotes changes in metabolic pathways available for obtaining energy. This metabolic reprogramming promotes a strong neuroprotective microglial response, which is less energetically demanding and is the result of the acquisition and maintenance of an anti-inflammatory phenotype. In our model, metabolic reprogramming not only prevents neurotoxicity, but also produces neuroprotection. As such, our work establishes a solid foundation to explore the pharmacological manipulation of Hv1 as an effective strategy for microglia reprogramming to promote neuroprotection in neurodegenerative disorders.

Abbreviations

2-aminobenzimidazole	ABI
2-guanidinobenzimidazole	2GBI
3-(2-amino-5-methyl-1H-imidazol-4-yl)-1-difluorophenyl	HIF
5-chloro-2-guanidinobenzimidazole	ClGBI
Bovine serum albumin	BSA
Days in vitro	DIV
Dizocilpine hydrogen maleate	MK801
Ethanediyl bis 6-methoxy-phenol manganese complex	EUK134
Extracellular pH	pH_e
Extracellular lactate	$Lactate_e$
Fetal bovine serum	FBS
Gamma interferon	IFNγ
Hank's Buffer with HEPES solution	HHBS
Highly aggressively proliferating immortalized	HAPI
Hydrogen voltage gated channel 1	Hv1
Interleukin 1β	IL-1β
Interleukin 4	IL-4
Interleukin 6	IL-6
Interleukin 10	IL-10
Intracellular Lactate	$Lactate_i$
Intracellular pH	pH_i
Lactate Dehydrogenase	LDH
Lipopolysaccharide	LPS
Neutralizing antibody of IL-10	nIL-10
Neutralizing antibody of TNF-α	TNF-α nAb
Neutralizing antibody of IL-6	IL-6 nAb
Nicotinamide adenine dinucleotide phosphate reduced	NADPH
Nitric oxide synthase	NOS
NADPH oxidases	NOX

NADPH oxidase 2	NOX2
Nicotinamide adenine dinucleotide reduced	NADH
Optical density	OD
Patterns associated with damage	DAMPs
Patterns associated with pathogens	PAMPs
Phosphate buffered saline	PBS
Phosphate buffered saline and Tween 20	PBST
Protein kinase C	PKC
Reactive oxygen species	ROS
Relative Fluorescence units	RFU
Relative light units	RLU
Threo-β-Benzyloxyaspartic acid	TBOA
Tetrazolium compound inner salt	MTS
Transforming growth factor beta	TGF-β
Tumor necrosis factor alpha	TNFα
Voltage sensitive domain	VSD

Declarations

- Ethics approval and consent to participate: Animals and experimental procedures were approved by the IACUC of University of Pittsburgh
- Consent for publication: Not applicable
- Availability of data and materials: The datasets used and/or analyzed during the current study are available from the corresponding author upon reasonable request.
- Competing interests: The authors declare that they have no competing interests
- Funding: NIH grant NS0432577
- Authors' contributions: D.R.H.E. and E.A. were responsible for conception and design of the study, D.R.H.E. and M.G.S. for data acquisition, and D.R.H.E., J.R.G., and E.A. for data analysis and presentation. All authors contributed to drafting the text and preparing the figures and have approved the submitted manuscript.
- Acknowledgements: We thank Karen Hartnett-Scott for expert technical assistance. This work was funded by NIH grant NS0432577 to EA.
- Authors' information: Not applicable

References

1. Parkhurst CN, Gan WB. Microglia dynamics and function in the CNS. Curr Opin Neurobiol. 2010;20:595–600. doi:10.1016/j.conb.2010.07.002.
2. Harry GJ, Kraft AD. Neuroinflammation and microglia: considerations and approaches for neurotoxicity assessment. Expert Opin Drug Metab Toxicol. 2008;4:1265–77. doi:10.1517/17425255.4.10.1265.
3. Kigerl KA, de Rivero Vaccari JP, Dietrich WD, Popovich PG, Keane RW. Pattern recognition receptors and central nervous system repair. Exp Neurol. 2014;258:5–16. doi:10.1016/j.expneurol.2014.01.001.
4. Cherry JD, Olschowka JA, O'Banion MK, Neuroinflammation. and M2 microglia: the good, the bad, and the inflamed. J Neuroinflammation. 2014;11:98. doi:10.1186/1742-2094-11-98.
5. Kim CC, Nakamura MC, Hsieh CL. Brain trauma elicits non-canonical macrophage activation states. J Neuroinflammation. 2016;13:117. doi:10.1186/s12974-016-0581-z.
6. Barcia C, et al. IFN-gamma signaling, with the synergistic contribution of TNF-alpha, mediates cell specific microglial and astroglial activation in experimental models of Parkinson's disease. Cell Death Dis. 2011;2:e142. doi:10.1038/cddis.2011.17.
7. Brown GC, Neher JJ. Eaten alive! Cell death by primary phagocytosis: 'phagoptosis'. Trends Biochem Sci. 2012;37:325–32. doi:10.1016/j.tibs.2012.05.002.
8. Aderem A, Underhill DM. Mechanisms of phagocytosis in macrophages. Annu Rev Immunol. 1999;17:593–623. doi:10.1146/annurev.immunol.17.1.593.
9. Kawasaki T, Kawai T. Toll-like receptor signaling pathways. Front Immunol. 2014;5:461. doi:10.3389/fimmu.2014.00461.
10. Dheen ST, Kaur C, Ling EA. Microglial activation and its implications in the brain diseases. Curr Med Chem. 2007;14:1189–97. doi:10.2174/092986707780597961.
11. Brown GC, Vilalta A. How microglia kill neurons. Brain Res. 2015;1628:288–97. doi:10.1016/j.brainres.2015.08.031.
12. Lue LF, Kuo YM, Beach T, Walker DG. Microglia activation and anti-inflammatory regulation in Alzheimer's disease. Mol Neurobiol. 2010;41:115–28. doi:10.1007/s12035-010-8106-8.
13. Andreou KE, et al. Anti-inflammatory Microglia/Macrophages As a Potential Therapeutic Target in Brain Metastasis. Front Oncol. 2017;7:251. doi:10.3389/fonc.2017.00251.
14. Stoll G, Jander S, Schroeter M. Cytokines in CNS disorders: neurotoxicity versus neuroprotection. J Neural Transm Suppl. 2000;59:81–9. doi:10.1007/978-3-7091-6781-6_11.
15. Hellwig S, Heinrich A, Biber K. The brain's best friend: microglial neurotoxicity revisited. Front Cell Neurosci. 2013;7:71. doi:10.3389/fncel.2013.00071.
16. Orihuela R, McPherson CA, Harry GJ. Microglial M1/M2 polarization and metabolic states. Br J Pharmacol. 2016;173:649–65. doi:10.1111/bph.13139.

17. Stratoulias V, Venero JL, Tremblay ME, Joseph B. Microglial subtypes: diversity within the microglial community. EMBO J. 2019;38:e101997. doi:10.15252/embj.2019101997.
18. Hu X, et al. Microglial and macrophage polarization-new prospects for brain repair. Nat Rev Neurol. 2015;11:56–64. doi:10.1038/nrneurol.2014.207.
19. Nair S, et al. Lipopolysaccharide-induced alteration of mitochondrial morphology induces a metabolic shift in microglia modulating the inflammatory response in vitro and in vivo. Glia. 2019;67:1047–61. doi:10.1002/glia.23587.
20. Bernier LP, et al. Nanoscale Surveillance of the Brain by Microglia via cAMP-Regulated Filopodia. *Cell Rep* **27**, 2895–2908 e2894, doi:10.1016/j.celrep.2019.05.010 (2019).
21. Volobouеva LA, Emery JF, Sun X, Giffard RG. Inflammatory response of microglial BV-2 cells includes a glycolytic shift and is modulated by mitochondrial glucose-regulated protein 75/mortalin. FEBS Lett. 2013;587:756–62. doi:10.1016/j.febslet.2013.01.067.
22. Wang L, et al. Glucose transporter 1 critically controls microglial activation through facilitating glycolysis. Mol Neurodegener. 2019;14:2. doi:10.1186/s13024-019-0305-9.
23. Ghosh S, Castillo E, Frias ES, Swanson RA. Bioenergetic regulation of microglia. Glia. 2018;66:1200–12. doi:10.1002/glia.23271.
24. Jha MK, Morrison BM. Lactate Transporters Mediate Glia-Neuron Metabolic Crosstalk in Homeostasis and Disease. Front Cell Neurosci. 2020;14:589582. doi:10.3389/fncel.2020.589582.
25. Persson M, Sandberg M, Hansson E, Ronnback L. Microglial glutamate uptake is coupled to glutathione synthesis and glutamate release. Eur J Neurosci. 2006;24:1063–70. doi:10.1111/j.1460-9568.2006.04974.x.
26. Suzuki C, et al. Differences in in vitro microglial accumulation of the energy metabolism tracers [(18)F]FDG and [(18)F]BCPP-EF during LPS- and IL4 stimulation. Sci Rep. 2021;11:13200. doi:10.1038/s41598-021-92436-0.
27. Gras G, Porcheray F, Samah B, Leone C. The glutamate-glutamine cycle as an inducible, protective face of macrophage activation. J Leukoc Biol. 2006;80:1067–75. doi:10.1189/jlb.0306153.
28. Liu Y, et al. Activation of microglia depends on Na+/H + exchange-mediated H + homeostasis. J Neurosci. 2010;30:15210–20. doi:10.1523/JNEUROSCI.3950-10.2010.
29. Li Y, et al. The voltage-gated proton channel Hv1 plays a detrimental role in contusion spinal cord injury via extracellular acidosis-mediated neuroinflammation. Brain Behav Immun. 2021;91:267–83. doi:10.1016/j.bbi.2020.10.005.
30. Wu LJ. Microglial voltage-gated proton channel Hv1 in ischemic stroke. Transl Stroke Res. 2014;5:99–108. doi:10.1007/s12975-013-0289-7.
31. Morgan D, et al. Voltage-gated proton channels maintain pH in human neutrophils during phagocytosis. Proc Natl Acad Sci U S A. 2009;106:18022–7. doi:10.1073/pnas.0905565106.
32. Sekar P, Huang DY, Chang SF, Lin WW. Coordinate effects of P2X7 and extracellular acidification in microglial cells. Oncotarget. 2018;9:12718–31. doi:10.18632/oncotarget.24331.

33. Faff L, Ohlemeyer C, Kettenmann H. Intracellular pH regulation in cultured microglial cells from mouse brain. *J Neurosci Res* **46**, 294–304, doi:10.1002/(SICI)1097-4547(19961101)46:3<294::AID-JNR2>3.0.CO;2-F (1996).
34. Nauseef WM. The phagocyte NOX2 NADPH oxidase in microbial killing and cell signaling. Curr Opin Immunol. 2019;60:130–40. doi:10.1016/j.coi.2019.05.006.
35. Li H, et al. Using ROS as a Second Messenger, NADPH Oxidase 2 Mediates Macrophage Senescence via Interaction with NF-kappaB during Pseudomonas aeruginosa Infection. *Oxid Med Cell Longev* 2018, 9741838, doi:10.1155/2018/9741838 (2018).
36. Zeng X, et al. Gp91phox (NOX2) in Activated Microglia Exacerbates Neuronal Damage Induced by Oxygen Glucose Deprivation and Hyperglycemia in an in Vitro Model. Cell Physiol Biochem. 2018;50:783–97. doi:10.1159/000494243.
37. Hernandez-Espinosa DR, Massieu L, Montiel T, Moran J. Role of NADPH oxidase-2 in the progression of the inflammatory response secondary to striatum excitotoxic damage. J Neuroinflammation. 2019;16:91. doi:10.1186/s12974-019-1478-4.
38. El Chemaly A, et al. VSOP/Hv1 proton channels sustain calcium entry, neutrophil migration, and superoxide production by limiting cell depolarization and acidification. J Exp Med. 2010;207:129–39. doi:10.1084/jem.20091837.
39. Kawai T, et al. Unconventional role of voltage-gated proton channels (VSOP/Hv1) in regulation of microglial ROS production. J Neurochem. 2017;142:686–99. doi:10.1111/jnc.14106.
40. Ramsey IS, Ruchti E, Kaczmarek JS, Clapham DE. Hv1 proton channels are required for high-level NADPH oxidase-dependent superoxide production during the phagocyte respiratory burst. Proc Natl Acad Sci U S A. 2009;106:7642–7. doi:10.1073/pnas.0902761106.
41. Ritzel RM, et al. Proton extrusion during oxidative burst in microglia exacerbates pathological acidosis following traumatic brain injury. Glia. 2021;69:746–64. doi:10.1002/glia.23926.
42. Lishko PV, Botchkina IL, Fedorenko A, Kirichok Y. Acid extrusion from human spermatozoa is mediated by flagellar voltage-gated proton channel. Cell. 2010;140:327–37. doi:10.1016/j.cell.2009.12.053.
43. Ramsey IS, Moran MM, Chong JA, Clapham DE. A voltage-gated proton-selective channel lacking the pore domain. Nature. 2006;440:1213–6. doi:10.1038/nature04700.
44. Musset B, et al. Zinc inhibition of monomeric and dimeric proton channels suggests cooperative gating. J Physiol. 2010;588:1435–49. doi:10.1113/jphysiol.2010.188318.
45. Hong L, Singh V, Wulff H, Tombola F. Interrogation of the intersubunit interface of the open Hv1 proton channel with a probe of allosteric coupling. Sci Rep. 2015;5:14077. doi:10.1038/srep14077.
46. Tian DS, et al. Deficiency in the voltage-gated proton channel Hv1 increases M2 polarization of microglia and attenuates brain damage from photothrombotic ischemic stroke. J Neurochem. 2016;139:96–105. doi:10.1111/jnc.13751.
47. Zhang ZJ, et al. Aging alters Hv1-mediated microglial polarization and enhances neuroinflammation after peripheral surgery. CNS Neurosci Ther. 2020;26:374–84. doi:10.1111/cns.13271.

48. Yu Y, et al. Microglial Hv1 proton channels promote white matter injuries after chronic hypoperfusion in mice. J Neurochem. 2020;152:350–67. doi:10.1111/jnc.14925.
49. Hong L, Kim IH, Tombola F. Molecular determinants of Hv1 proton channel inhibition by guanidine derivatives. Proc Natl Acad Sci U S A. 2014;111:9971–6. doi:10.1073/pnas.1324012111.
50. Zhao C, et al. HIFs: New arginine mimic inhibitors of the Hv1 channel with improved VSD-ligand interactions. J Gen Physiol 153, doi:10.1085/jgp.202012832 (2021).
51. Ma J, et al. The HVCN1 voltage-gated proton channel contributes to pH regulation in canine ventricular myocytes. J Physiol. 2022. doi:10.1113/JP282126.
52. Meszaros B, et al. The voltage-gated proton channel hHv1 is functionally expressed in human chorion-derived mesenchymal stem cells. Sci Rep. 2020;10:7100. doi:10.1038/s41598-020-63517-3.
53. Asuaje A, et al. The inhibition of voltage-gated H(+) channel (HVCN1) induces acidification of leukemic Jurkat T cells promoting cell death by apoptosis. Pflugers Arch. 2017;469:251–61. doi:10.1007/s00424-016-1928-0.
54. Lim VT, Freites JA, Tombola F, Tobias DJ. Thermodynamics and Mechanism of the Membrane Permeation of Hv1 Channel Blockers. J Membr Biol. 2021;254:5–16. doi:10.1007/s00232-020-00149-8.
55. Cheepsunthorn P, Radov L, Menzies S, Reid J, Connor JR. Characterization of a novel brain-derived microglial cell line isolated from neonatal rat brain. Glia. 2001;35:53–62. doi:10.1002/glia.1070.
56. Hartnett KA, et al. NMDA receptor-mediated neurotoxicity: a paradoxical requirement for extracellular Mg2 + in Na+/Ca2+-free solutions in rat cortical neurons in vitro. J Neurochem. 1997;68:1836–45. doi:10.1046/j.1471-4159.1997.68051836.x.
57. Saura J, Tusell JM, Serratosa J. High-yield isolation of murine microglia by mild trypsinization. Glia. 2003;44:183–9. doi:10.1002/glia.10274.
58. Hayes MP, Freeman SL, Donnelly RP. IFN-gamma priming of monocytes enhances LPS-induced TNF production by augmenting both transcription and MRNA stability. Cytokine. 1995;7:427–35. doi:10.1006/cyto.1995.0058.
59. Zhang SC, Fedoroff S. Neuron-microglia interactions in vitro. Acta Neuropathol. 1996;91:385–95. doi:10.1007/s004010050440.
60. Aras MA, Hartnett KA, Aizenman E. Assessment of cell viability in primary neuronal cultures. *Curr Protoc Neurosci Chap. 7*, Unit 7 18, doi:10.1002/0471142301.ns0718s44 (2008).
61. Justice JA, et al. Molecular Neuroprotection Induced by Zinc-Dependent Expression of Hepatitis C-Derived Protein NS5A Targeting Kv2.1 Potassium Channels. J Pharmacol Exp Ther. 2018;367:348–55. doi:10.1124/jpet.118.252338.
62. Yeh CY, et al. Targeting a Potassium Channel/Syntaxin Interaction Ameliorates Cell Death in Ischemic Stroke. J Neurosci. 2017;37:5648–58. doi:10.1523/JNEUROSCI.3811-16.2017.
63. Schulien AJ, et al. Targeted disruption of Kv2.1-VAPA association provides neuroprotection against ischemic stroke in mice by declustering Kv2.1 channels. Sci Adv 6, doi:10.1126/sciadv.aaz8110

(2020).

64. Buttke TM, McCubrey JA, Owen TC. Use of an aqueous soluble tetrazolium/formazan assay to measure viability and proliferation of lymphokine-dependent cell lines. J Immunol Methods. 1993;157:233–40. doi:10.1016/0022-1759(93)90092-I.
65. Duellman SJ, et al. Bioluminescent, Nonlytic, Real-Time Cell Viability Assay and Use in Inhibitor Screening. Assay Drug Dev Technol. 2015;13:456–65. doi:10.1089/adt.2015.669.
66. Pal S, Hartnett KA, Nerbonne JM, Levitan ES, Aizenman E. Mediation of neuronal apoptosis by Kv2.1-encoded potassium channels. J Neurosci. 2003;23:4798–802. doi:10.1523/jneurosci.23-12-04798.2003.
67. Knoch ME, Hartnett KA, Hara H, Kandler K, Aizenman E. Microglia induce neurotoxicity via intraneuronal Zn(2+) release and a K(+) current surge. Glia. 2008;56:89–96. doi:10.1002/glia.20592.
68. Dimayuga FO, et al. SOD1 overexpression alters ROS production and reduces neurotoxic inflammatory signaling in microglial cells. J Neuroimmunol. 2007;182:89–99. doi:10.1016/j.jneuroim.2006.10.003.
69. Zhao YY, Yan DJ, Chen ZW. Role of AIF-1 in the regulation of inflammatory activation and diverse disease processes. Cell Immunol. 2013;284:75–83. doi:10.1016/j.cellimm.2013.07.008.
70. Lian H, Roy E, Zheng H. Microglial Phagocytosis Assay. Bio Protoc 6, doi:10.21769/BioProtoc.1988 (2016).
71. Minkenberg I, Ferber E. Lucigenin-dependent chemiluminescence as a new assay for NAD(P)H-oxidase activity in particulate fractions of human polymorphonuclear leukocytes. J Immunol Methods. 1984;71:61–7. doi:10.1016/0022-1759(84)90206-0.
72. Veremeyko T, Yung AWY, Anthony DC, Strekalova T, Ponomarev ED. Early Growth Response Gene-2 Is Essential for M1 and M2 Macrophage Activation and Plasticity by Modulation of the Transcription Factor CEBPbeta. Front Immunol. 2018;9:2515. doi:10.3389/fimmu.2018.02515.
73. Ozkan P, Mutharasan R. A rapid method for measuring intracellular pH using BCECF-AM. Biochim Biophys Acta. 2002;1572:143–8. doi:10.1016/s0304-4165(02)00303-3.
74. Ilina EI, et al. Effects of soluble CPE on glioma cell migration are associated with mTOR activation and enhanced glucose flux. Oncotarget. 2017;8:67567–91. doi:10.18632/oncotarget.18747.
75. Vidugiriene J, et al. Bioluminescent cell-based NAD(P)/NAD(P)H assays for rapid dinucleotide measurement and inhibitor screening. Assay Drug Dev Technol. 2014;12:514–26. doi:10.1089/adt.2014.605.
76. Datki ZL, Hunya A, Penke B. A novel and simple fluorescence method for the measurement of presynaptic vesicular zinc release in acute hippocampal slices with a fluorescence plate reader. Brain Res Bull. 2007;74:183–7. doi:10.1016/j.brainresbull.2007.06.001.
77. Gao H, Dai W, Zhao L, Min J, Wang F The Role of Zinc and Zinc Homeostasis in Macrophage Function. *J Immunol Res* 2018, 6872621, doi:10.1155/2018/6872621 (2018).

78. Wu LJ. Voltage-gated proton channel HV1 in microglia. Neuroscientist. 2014;20:599–609. doi:10.1177/1073858413519864.
79. Hirano K, et al. Discovery of GSK2795039, a Novel Small Molecule NADPH Oxidase 2 Inhibitor. Antioxid Redox Signal. 2015;23:358–74. doi:10.1089/ars.2014.6202.
80. Lam TI, et al. Intracellular pH reduction prevents excitotoxic and ischemic neuronal death by inhibiting NADPH oxidase. Proc Natl Acad Sci U S A. 2013;110:E4362–8. doi:10.1073/pnas.1313029110.
81. Busa WB, Nuccitelli R. Metabolic regulation via intracellular pH. Am J Physiol. 1984;246:R409–38. doi:10.1152/ajpregu.1984.246.4.R409.
82. Song S, et al. Elevated microglial oxidative phosphorylation and phagocytosis stimulate post-stroke brain remodeling and cognitive function recovery in mice. Commun Biol. 2022;5:35. doi:10.1038/s42003-021-02984-4.
83. Lauro C, Limatola C. Metabolic Reprograming of Microglia in the Regulation of the Innate Inflammatory Response. Front Immunol. 2020;11:493. doi:10.3389/fimmu.2020.00493.
84. Winkler U, Hirrlinger J. Crosstalk of Signaling and Metabolism Mediated by the NAD(+)/NADH Redox State in Brain Cells. Neurochem Res. 2015;40:2394–401. doi:10.1007/s11064-015-1526-0.
85. Baik SH, et al. A Breakdown in Metabolic Reprogramming Causes Microglia Dysfunction in Alzheimer's Disease. *Cell Metab* **30**, 493–507 e496, doi:10.1016/j.cmet.2019.06.005 (2019).
86. Islam A, et al. Sustained anti-inflammatory effects of TGF-β1 on microglia/macrophages. Biochim Biophys Acta Mol Basis Dis. 2018;1864:721–34. doi:10.1016/j.bbadis.2017.12.022.
87. Fernandez-Arjona MDM, Grondona JM, Granados-Duran P, Fernandez-Llebrez P, Lopez-Avalos MD. Microglia Morphological Categorization in a Rat Model of Neuroinflammation by Hierarchical Cluster and Principal Components Analysis. Front Cell Neurosci. 2017;11:235. doi:10.3389/fncel.2017.00235.
88. Simpson DSA, Oliver PL. ROS Generation in Microglia: Understanding Oxidative Stress and Inflammation in Neurodegenerative Disease. Antioxid (Basel). 2020;9:743. doi:10.3390/antiox9080743.
89. Rong Y, Doctrow SR, Tocco G, Baudry M. EUK-134, a synthetic superoxide dismutase and catalase mimetic, prevents oxidative stress and attenuates kainate-induced neuropathology. Proc Natl Acad Sci U S A. 1999;96:9897–902. doi:10.1073/pnas.96.17.9897.
90. He K, Aizenman E. ERK signaling leads to mitochondrial dysfunction in extracellular zinc-induced neurotoxicity. J Neurochem. 2010;114:452–61. doi:10.1111/j.1471-4159.2010.06762.x.
91. Pan E, et al. Vesicular zinc promotes presynaptic and inhibits postsynaptic long-term potentiation of mossy fiber-CA3 synapse. Neuron. 2011;71:1116–26. doi:10.1016/j.neuron.2011.07.019.
92. Liu B, et al. The RNase MCPIP3 promotes skin inflammation by orchestrating myeloid cytokine response. Nat Commun. 2021;12:4105. doi:10.1038/s41467-021-24352-w.

93. Muendlein HI, et al. ZBP1 promotes LPS-induced cell death and IL-1beta release via RHIM-mediated interactions with RIPK1. Nat Commun. 2021;12:86. doi:10.1038/s41467-020-20357-z.
94. Jantaratnotai N, Utaisincharoen P, Piyachaturawat P, Chongthammakun S, Sanvarinda Y. Inhibitory effect of Curcuma comosa on NO production and cytokine expression in LPS-activated microglia. Life Sci. 2006;78:571–7. doi:10.1016/j.lfs.2005.04.065.
95. Stefano GB, et al. Nitric oxide modulates microglial activation. Med Sci Monit. 2004;10:BR17–22.
96. Jiang X, Yi S, Liu Q, Zhang J. The secretome of M1 and M2 microglia differently regulate proliferation, differentiation and survival of adult neural stem/progenitor cell. *bioRxiv*, 2021.2009.2015.460424, doi:10.1101/2021.09.15.460424 (2021).
97. Smith JA, Das A, Ray SK, Banik NL. Role of pro-inflammatory cytokines released from microglia in neurodegenerative diseases. Brain Res Bull. 2012;87:10–20. doi:10.1016/j.brainresbull.2011.10.004.
98. Kettenmann H, Hanisch UK, Noda M, Verkhratsky A. Physiology of microglia. Physiol Rev. 2011;91:461–553. doi:10.1152/physrev.00011.2010.
99. Decoursey TE. Voltage-gated proton channels. Compr Physiol. 2012;2:1355–85. doi:10.1002/cphy.c100071.
100. Kawai T, Tatsumi S, Kihara S, Sakimura K, Okamura Y. Mechanistic insight into the suppression of microglial ROS production by voltage-gated proton channels (VSOP/Hv1). Channels (Austin). 2018;12:1–8. doi:10.1080/19336950.2017.1385684.
101. Takeda H, Yamaguchi T, Yano H, Tanaka J. Microglial metabolic disturbances and neuroinflammation in cerebral infarction. J Pharmacol Sci. 2021;145:130–9. doi:10.1016/j.jphs.2020.11.007.
102. Chausse B, Kakimoto PA, Kann O. Microglia and lipids: how metabolism controls brain innate immunity. Semin Cell Dev Biol. 2021;112:137–44. doi:10.1016/j.semcdb.2020.08.001.
103. Bernier LP, York EM, MacVicar BA. Immunometabolism in the Brain: How Metabolism Shapes Microglial Function. Trends Neurosci. 2020;43:854–69. doi:10.1016/j.tins.2020.08.008.
104. Borst K, Schwabenland M, Prinz M. Microglia metabolism in health and disease. Neurochem Int. 2019;130:104331. doi:10.1016/j.neuint.2018.11.006.
105. Soto-Heredero G, Gomez de Las Heras MM, Gabande-Rodriguez E, Oller J, Mittelbrunn M. Glycolysis - a key player in the inflammatory response. FEBS J. 2020;287:3350–69. doi:10.1111/febs.15327.
106. Srivastava S. Emerging therapeutic roles for NAD(+) metabolism in mitochondrial and age-related disorders. Clin Transl Med. 2016;5:25. doi:10.1186/s40169-016-0104-7.
107. Rice AC, et al. Lactate administration attenuates cognitive deficits following traumatic brain injury. Brain Res. 2002;928:156–9. doi:10.1016/s0006-8993(01)03299-1.
108. Provenzano F, Perez MJ, Deleidi M. Redefining Microglial Identity in Health and Disease at Single-Cell Resolution. Trends Mol Med. 2021;27:47–59. doi:10.1016/j.molmed.2020.09.001.
109. Lannes N, Eppler E, Etemad S, Yotovski P, Filgueira L. Microglia at center stage: a comprehensive review about the versatile and unique residential macrophages of the central nervous system.

Oncotarget. 2017;8:114393–413. doi:10.18632/oncotarget.23106.

110. Kremlev SG, Roberts RL, Palmer C. Differential expression of chemokines and chemokine receptors during microglial activation and inhibition. J Neuroimmunol. 2004;149:1–9. doi:10.1016/j.jneuroim.2003.11.012.

111. Kremlev SG, Palmer C. Interleukin-10 inhibits endotoxin-induced pro-inflammatory cytokines in microglial cell cultures. J Neuroimmunol. 2005;162:71–80. doi:10.1016/j.jneuroim.2005.01.010.

112. Colombo E, Farina C, Astrocytes. Key Regulators of Neuroinflammation. Trends Immunol. 2016;37:608–20. doi:10.1016/j.it.2016.06.006.

Figures

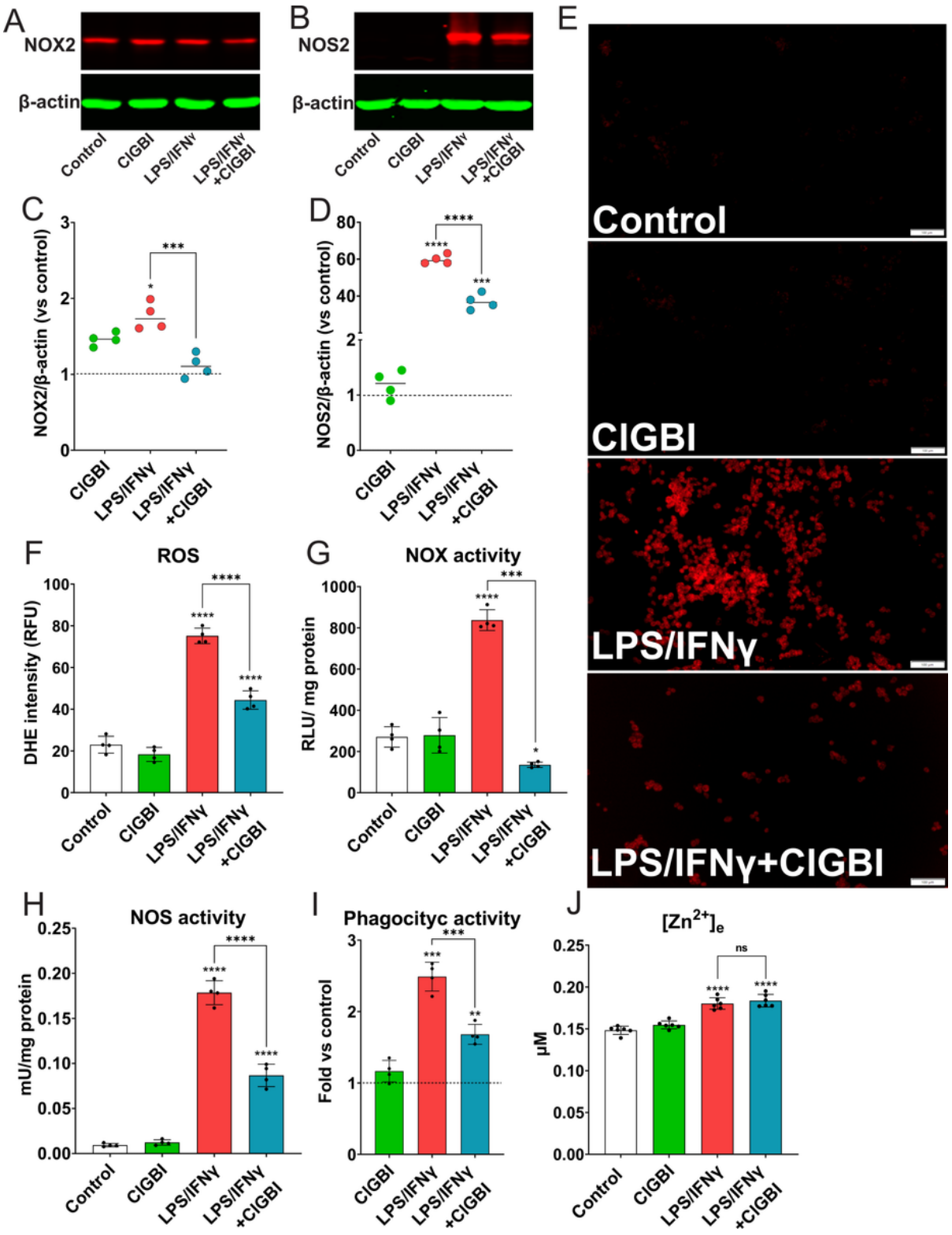

Figure 1

Hv1 inhibition hampers the inflammatory activation profile of HAPI cells. Representative Western blot images for NOX2 ***(A)*** and NOS2 ***(B)***; β-actin was used as a loading control. Quantification of protein bands for NOX2/β-actin ***(C)*** *(n=4)* and NOS2/β-actin ***(C)*** *(n=4)*. ***E)*** ROS detection. Representative micrographs of cells stained with DhE (red mark). Fields were randomly selected, paired based on cell density, and the image was then captured at 10x (scale bar=100μm). ***F)*** Quantification of end point DhE

fluorescence *(n=4)*. Data are expressed in relative fluorescence units (RFU). ***G)*** NOX activity determination by the resulting luminescence from lucigenin oxidation after the addition of NADPH. Data are expressed as relative light units (RLU) per mg of protein *(n=4)*. ***H)*** Determination of NOS activity by colorimetry linked to nitric oxide production. Data are presented as one mU per milligram of protein *(n=4)*. ***I)*** Determination of phagocytic activity by quantifying the fluorescence intensity of internalized pre-labeled green *E. coli (n=4)*. ***J)*** Determination of extracellular zinc by FluoZin3; results are expressed in µM based on a standard concentration curve of $ZnCl_2$ in a Chelex-treated solution *(n=6)*. All values displayed represent the mean ± SEM of at least four independent experiments, each performed in triplicate. Graphs comparing values across groups were analyzed via one-way ANOVA with Tukey post-hoc analysis for individual comparisons. Unspecified comparisons in F-J are vs. control. Unspecified comparisons in **C**, **D**, and **I** vs. normalized controls (dashed lines) were separately analyzed via one sample t tests vs. 1. Significance is shown as $^{*}p<0.05$ ** $p < 0.01$, *** $p < 0.005$ and **** $p < 0.001$.

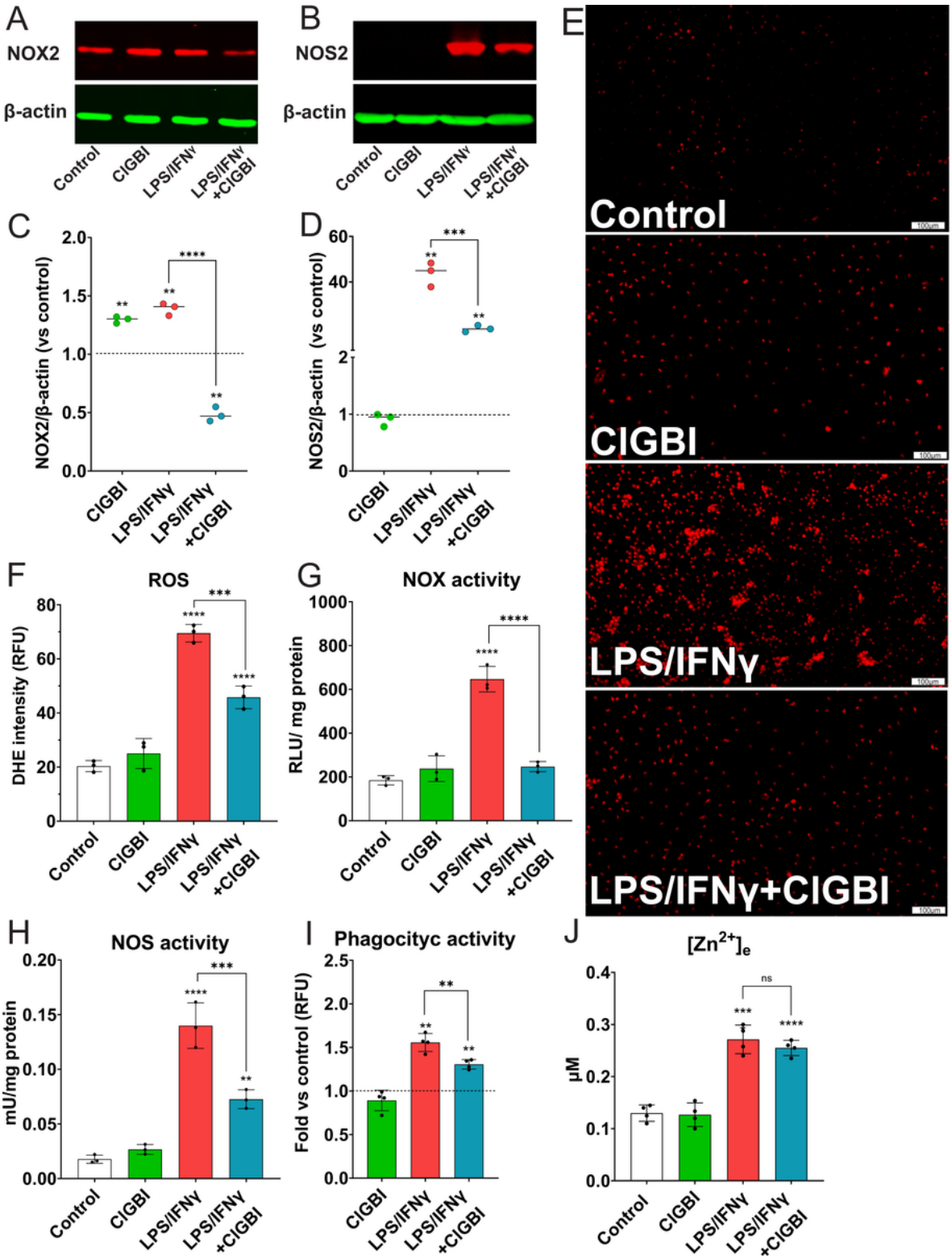

Figure 2

Hv1 inhibition also hampers the inflammatory activation profile of primary mouse microglia. See descriptions in Fig. 1 for individual panels. Essentially a similar response profile is observed in both HAPI cells and primary mouse microglial cells. All parameters measured are the same in Figs. 1 and 2. All values displayed represent the mean ± SEM of at least four independent experiments, each performed in triplicate. Graphs comparing values across groups were analyzed via one-way ANOVA with Tukey post-

hoc analysis for individual comparisons. Unspecified comparisons in F-J are vs. control. Unspecified comparisons in **C**, **D**, and I vs. normalized controls (dashed lines) were separately analyzed via one sample t tests vs. 1. Significance is shown as ** $p < 0.01$, *** $p < 0.005$ and **** $p < 0.001$.

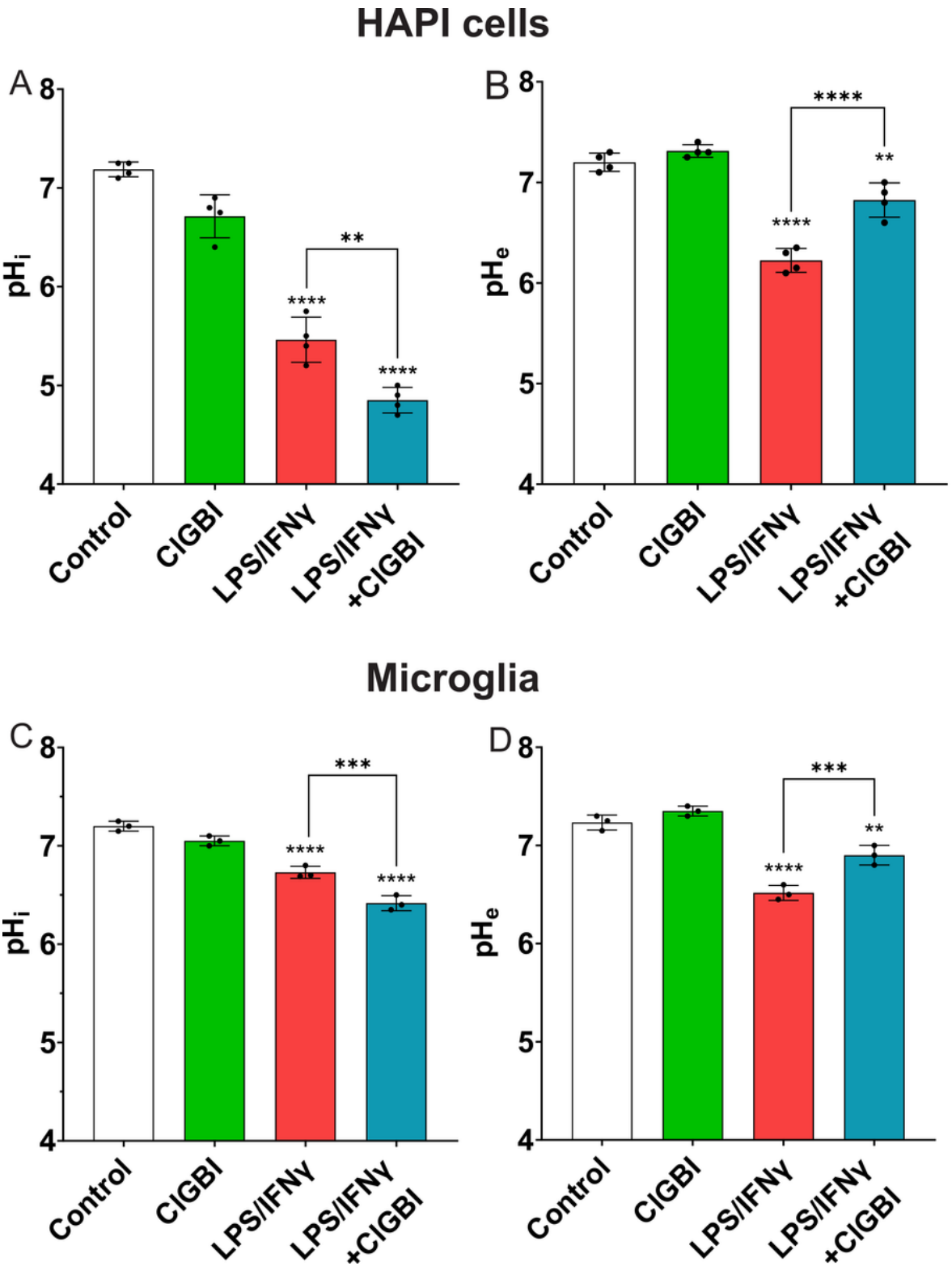

Figure 3

Hv1 block prevents proton extrusion and acidifies the intracellular pH of both activated HAPI cells and microglia. Comparison of the ***A)*** intracellular and ***B)*** extracellular pH of non-activated and activated HAPI cells treated with 10 μM ClGBI *(n=4)* denoting the increase in intracellular pH as well as increased extracellular pH_e in ClGBI-treated activated cells. Fluorometric determination of ***C)*** intracellular and ***D)*** extracellular pH of non-activated or activated microglia treated with or without 10 μM ClGBI *(n=4)*. pH measurements are based on calibrated BCFL-AM fluorescence. Extracellular pH was confirmed by a potentiometer. Data are expressed as units on the logarithmic pH scale and represented as mean ± SEM of at least four independent experiments done in triplicate. Graphs comparing values across groups were analyzed via one-way ANOVA with Tukey post-hoc analysis for individual comparisons. Unspecified comparisons in B-F are vs. control. Significance is shown as ** $p < 0.01$, *** $p < 0.005$ and **** $p < 0.001$.

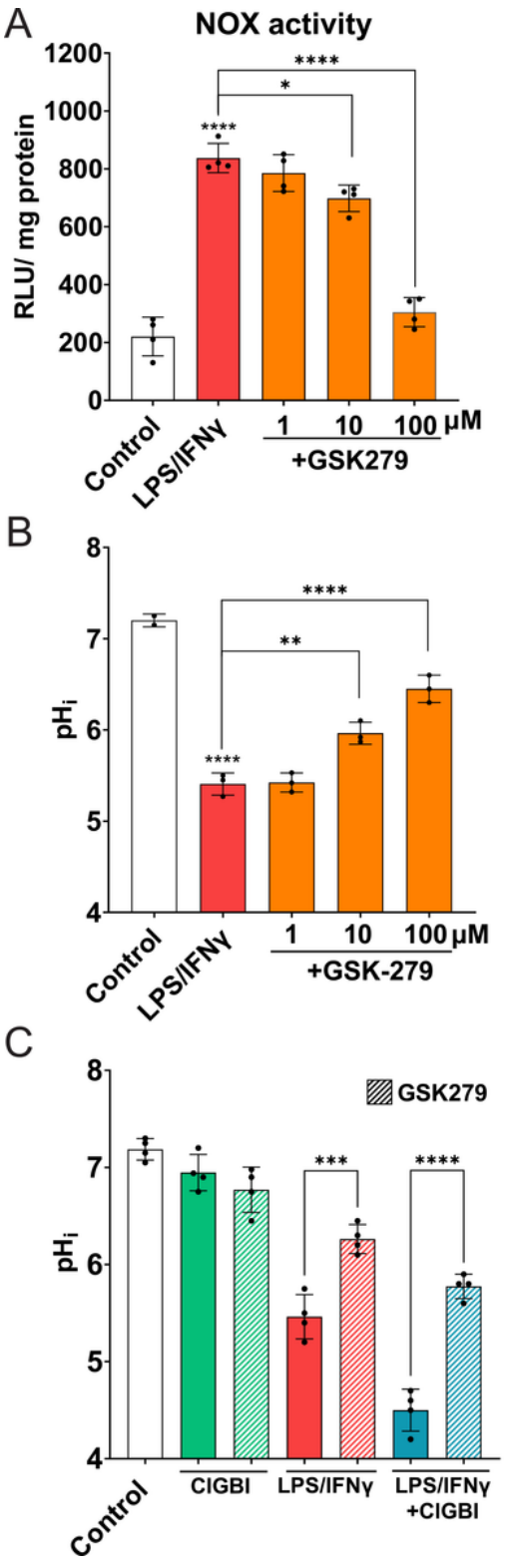

Figure 4

NOX2 activity promotes intracellular acidification in activated HAPI cells. ***A)*** Determination of NOX activity in activated HAPI cells in the presence of 1-100 μM GSK-279, an NOX2 inhibitor. Activity was obtained via quantification of luminescence resulting from the oxidation of lucigenin and expressed as relative light units (RLU) per mg of protein *(n=4)*. ***B)*** Fluorometric determination of intracellular pH in activated HAPI cells treated with 1-100 μM GSK-279. Values represents the detection of BCFL-AM and are

expressed as units on the logarithmic pH scale *(n=3)*. **C)** Comparation of fluorometric determination of intracellular pH in non-activated and activated HAPI cells treated with ClGBI (10 μM) and GSK279 (100μM; n=4). Results represents the detection of BCFL-AM and expressed as units on the logarithmic pH scale. All data are presented as Mean ± SEM of at least three independent experiments performed in triplicate. Analysis via one-way ANOVA with Tukey post-hoc analysis for individual comparisons. Unspecified comparisons in all panels are vs. control. Significance is shown as * $p < 0.05$, ** $p < 0.01$, *** $p < 0.005$ and **** $p < 0.001$.

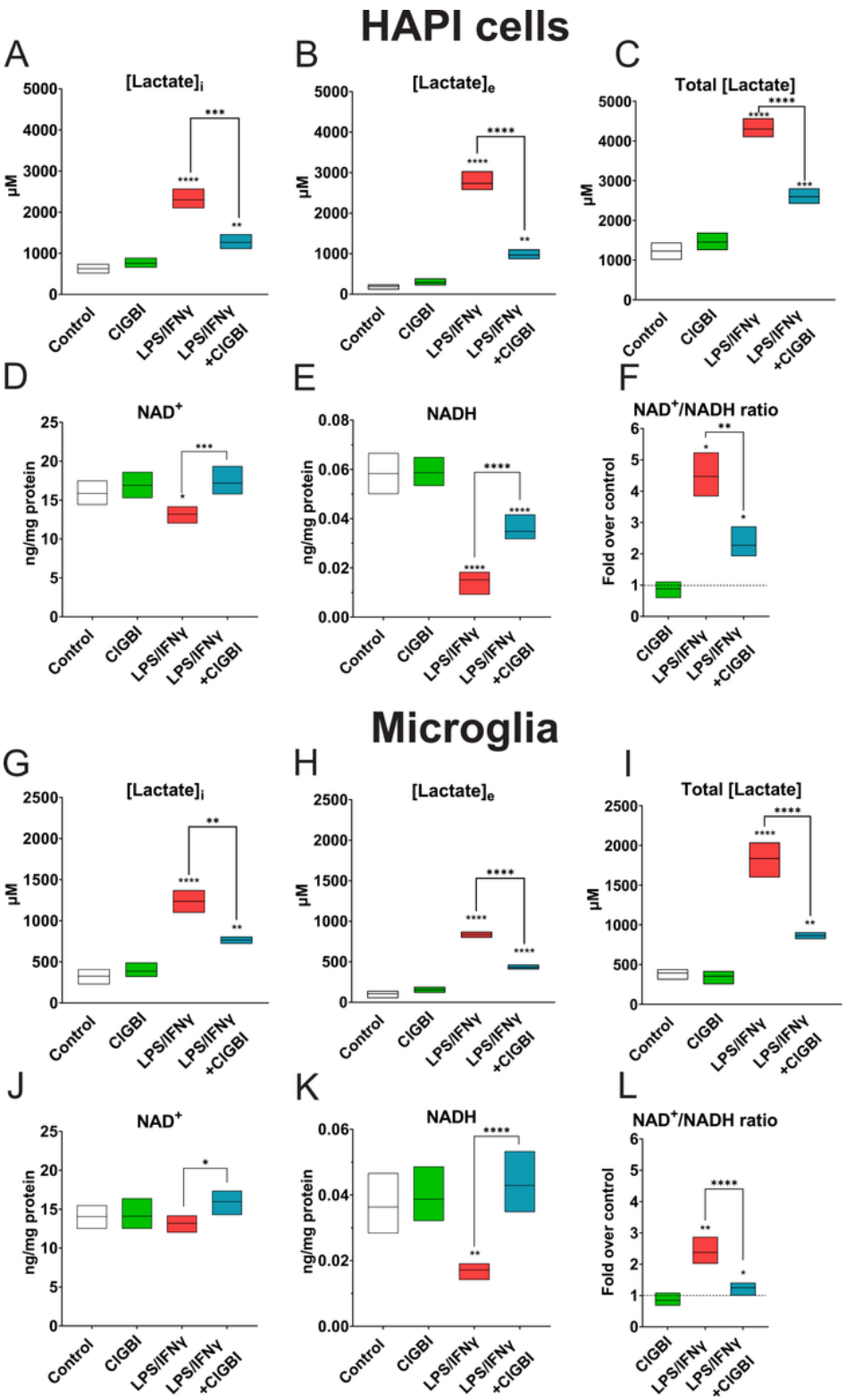

Figure 5

Pharmacological inhibition of Hv1 modifies the activation metabolic profile of HAPI cells and mouse microglial cells. Determination of intracellular, extracellular, and total lactate using a bioluminescence reductase/luciferase system in non-activated and activated HAPI cells ***(A-C)*** and mouse microglia ***(G-I)*** in the absence or presence of 10 µM ClGBI *(n=4)*. Data are expressed as lactate concentration (µM) based on a standard curve provided by the manufacturer. Measurement of NAD+ and NADH by a colorimetric

assay in non-activated and activated HAPI cells ***(D, E)*** and mouse microglia ***(J, K)*** in the absence and presence of 10 μM ClGBI, as well as the resulting NAD+/NADH ratios ***(F, L)***, which were normalized to control ratios (dotted line) *(n=4)*. Data in (**D**, **E**, **J**, **K**) are expressed as the concentration of NAD+ or NADH (ng per mg of protein) based on a curve provided by the manufacturer. The results are presented as the mean ± SEM of at least four independent experiments. Graphs comparing values across groups were analyzed via one-way ANOVA with Tukey post-hoc analysis for individual comparisons. Unspecified comparisons in **A**-**E** and G-K are vs. control. Unspecified comparisons in **F** and **L** to normalized controls (dashed lines) were separately analyzed via one sample t test vs. 1. Significance is shown as $^{*}p < 0.05$, $^{**}p < 0.01$, $^{***}p < 0.005$ and $^{****}p < 0.001$.

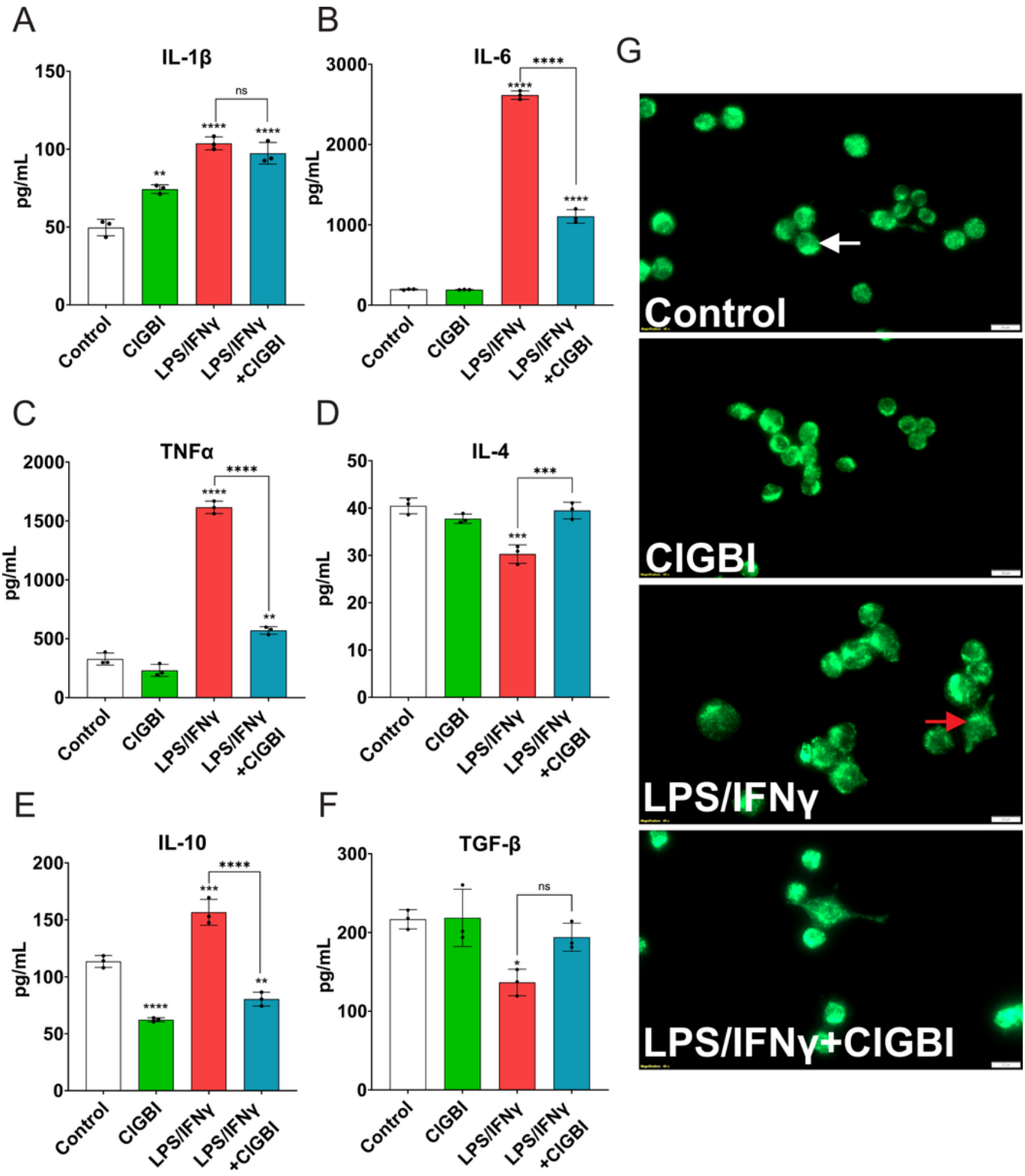

Figure 6

Hv1 inhibition promotes an anti-inflammatory HAPI cells activation phenotype. Determination of IL-1β, IL-6, TNFα, IL-4, IL-10 and TGF-β ***(A-F)*** by ELISA immunoassay in the culture medium of non-activated and activated HAPI cells in the presence of 10 μM ClGBI. Results are expressed as cytokine concentration per ml (pg/ml; n=3). ***G)*** Representative images obtained by immunocytochemistry (40x) of the morphology of non-activated (white arrow) and activated (red arrow) HAPI cells stained with Iba-1 (green) and DAPI

(blue). Scale bar = 20 μm. Results are presented as the mean ± SEM of 3 independent experiments, performed in triplicate. They were analyzed via one-way ANOVA with Tukey post-hoc analysis for individual comparisons. Unspecified comparisons are vs. control. Significance is shown as ** $p < 0.01$, *** $p < 0.005$ and **** $p < 0.001$.

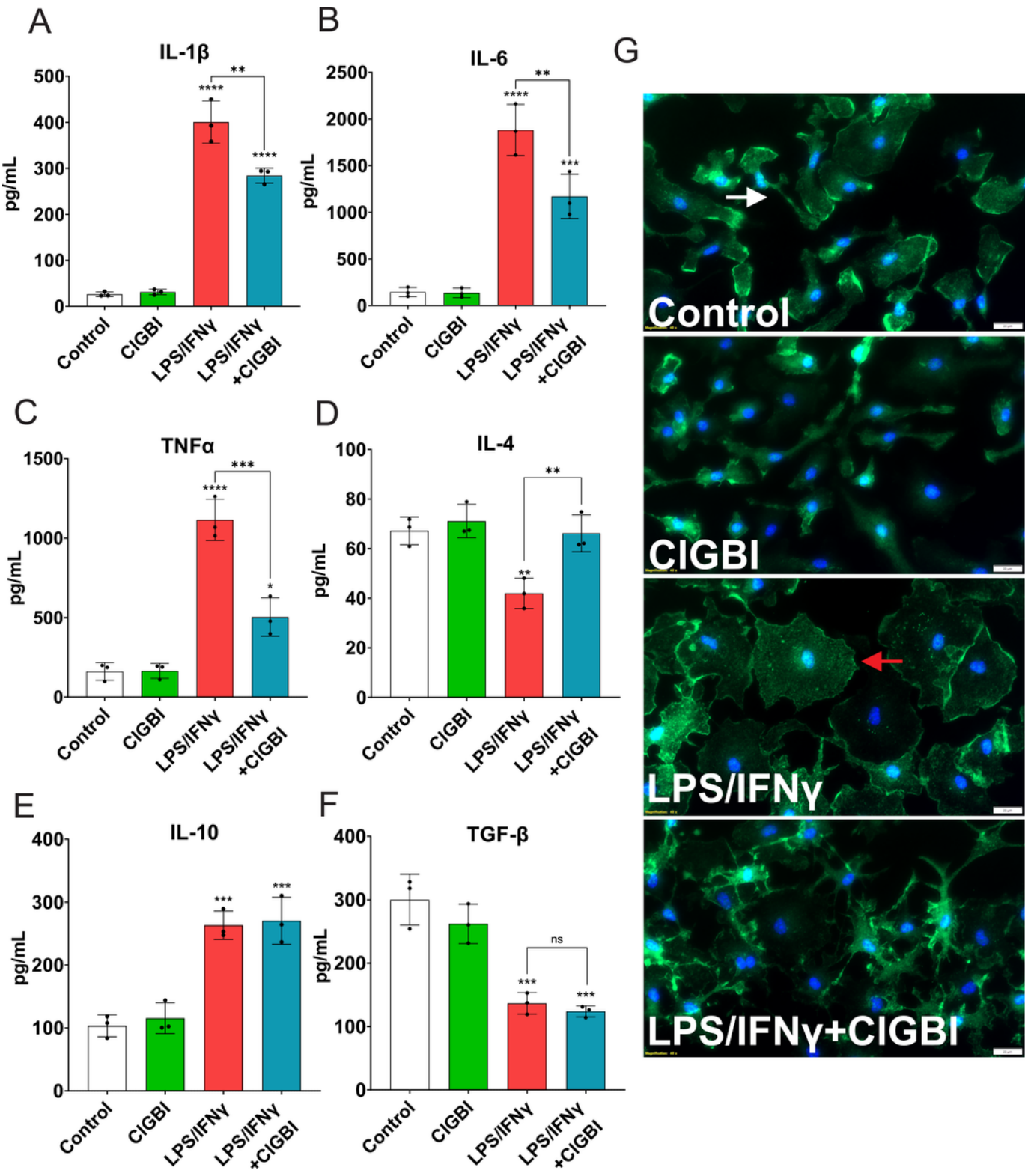

Figure 7

Hv1 inhibition also promotes an anti-inflammatory microglial activation phenotype. See descriptions in Fig. 6 for individual panels ***(A-F)***. Essentially a similar response profile is observed in both HAPI cells and primary mouse microglial cells. All parameters measured are the same in Figs. 6 and 7. ***G)*** Representative images obtained by immunocytochemistry (40x) of the morphology of non-activated (white arrow) and activated (red arrow) HAPI cells stained with Iba-1 (green) and DAPI (blue). Scale bar = 20 μm. Results are presented as the mean ± SEM of 3 independent experiments, performed in triplicate. They were analyzed via one-way ANOVA with Tukey post-hoc analysis for individual comparisons. Unspecified comparisons are vs. control. Significance is shown as * $p < 0.05$, ** $p < 0.01$, *** $p < 0.005$ and **** $p < 0.001$.

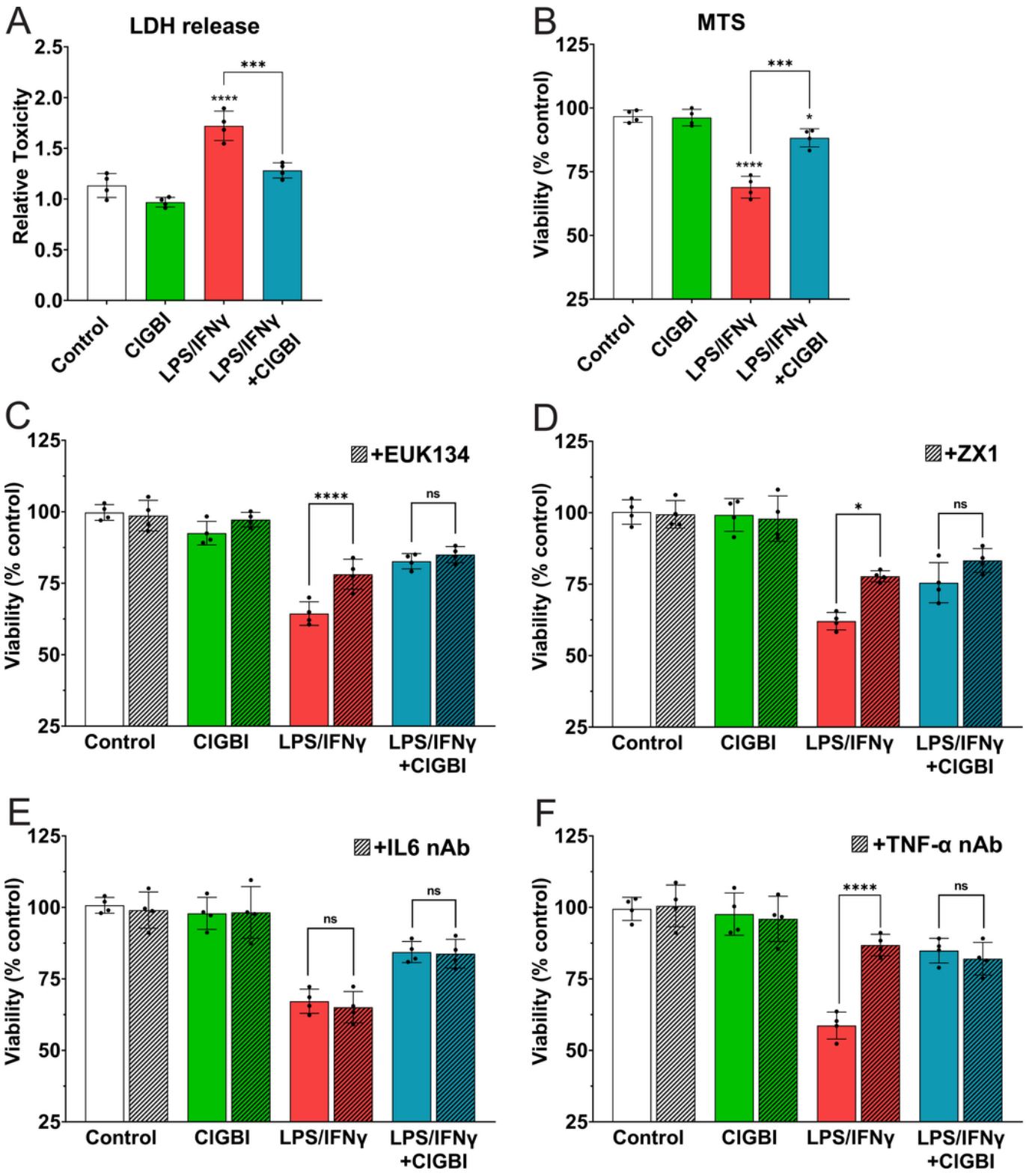

Figure 8

Hv1 inhibition during activation reduces HAPI cells inflammatory neurotoxicity. ***A)*** Toxicity evidenced by the LDH release from cortical neurons treated with conditioned medium from non-activated and activated HAPI cells in the absence and presence of 10 μM ClGBI *(n=4)*. ***B)*** Cortical neurons viability was also determined with, and MTS colorimetric assay of cortical cultures treated with HAPI cells conditioned medium as in A *(n=4)*. **(C-F)** Determination of specific neurotoxic components of the secretome trough

MTS assay of cortical cultures treated with conditioned medium and ***C)*** an antioxidant (100 μM EUK134), ***D)*** a membrane-permeant zinc chelator (5 μM ZX1), ***E)*** interleukin 6 neutralizing antibody (IL-6 nAb) and ***F)*** TNF-α neutralizing antibody (TNF-α nAb; n=4). Results were normalized to baseline LDH (A) or MTS (**B**-**F**) values from cells treated with HAPI cell medium that was never exposed to the HAPI cells themselves. Viability improved in EUK134, ZX1 and, especially, in TNF-α neutralizing antibody treated cells. Results are expressed as either relative LDH release (**A**), or percent viability as the mean ± SM of four independent experiments, each performed in triplicate. Data were analyzed via one-way ANOVA with Tukey post-hoc analysis for individual comparisons. Unspecified comparisons in A and B were vs. control. Significance is shown as * $p < 0.05$, *** $p < 0.005$ and **** $p < 0.001$.

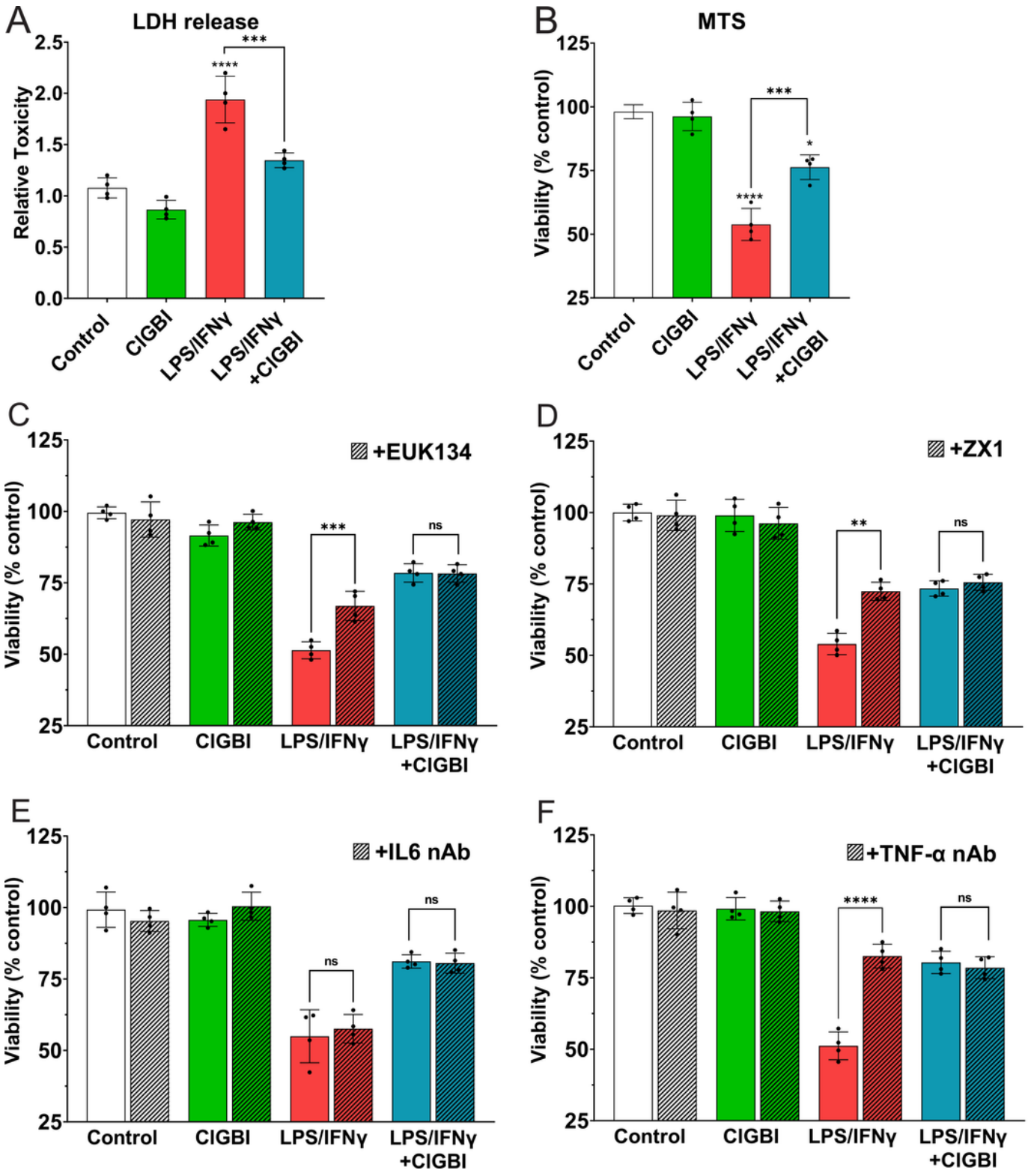

Figure 9

Hv1 inhibition during activation also reduces microglia inflammatory neurotoxicity. See descriptions in Fig. 8 for individual panels *(A-F)*. Essentially a similar response profile is observed in both HAPI cells and primary microglia cultures. All parameters measured are the same in Figs. 8 and 9. Once again, viability improved in EUK134, ZX1 and, especially, in TNF-α neutralizing antibody treated cells. Results are expressed as either relative LDH release (A), or percent viability as the mean ± SEM of four independent

experiments, each performed in triplicate. Data were analyzed via one-way ANOVA with Tukey post-hoc analysis for individual comparisons. Unspecified comparisons in A and B were vs. control. Significance is shown as ** $p < 0.01$, *** $p < 0.005$ and **** $p < 0.001$.

Supplementary Files

This is a list of supplementary files associated with this preprint. Click to download.

- Graphicalabstract.pdf
- Supp.FigureS1.pdf
- Supp.FigureS2.pdf
- Supp.FigureS3.pdf
- Supp.FigureS4.pdf
- Supp.FigureS5.pdf
- Supp.FigureS6.pdf
- Supp.FigureS7.pdf